

Optimal Targeting in Dynamic Systems

Yuchen Hu
MIT

Shuangning Li
University of Chicago

Stefan Wager
Stanford University

Draft version June 2026

Abstract

Modern treatment targeting methods often rely on estimating a conditional average treatment effect (CATE) using machine learning tools. While effective in identifying who benefits from treatment on the individual level, these approaches typically overlook system-level dynamics that may arise when treatments induce strain on shared capacity. We study the problem of targeting in Markovian systems, where treatment decisions must be made one at a time as units arrive, and early decisions can impact later outcomes through delayed or limited access to resources. We show that optimal policies in such settings compare CATE-like quantities to state-specific thresholds, where each threshold reflects the expected cumulative impact on the system of treating an additional individual in the given state. We propose an algorithm that augments standard CATE estimation with state-level value iteration to estimate these thresholds from observational data. Theoretical results establish consistency and convergence guarantees, and empirical studies demonstrate that our method improves long-run outcomes considerably relative to individual-level CATE targeting rules and generic offline reinforcement learning algorithms.

1 Introduction

Flexible machine-learning-based causal inference tools are widely used to guide decision-making and treatment prioritization rules across various domains. The conditional average treatment effect (CATE), which quantifies the expected benefit of treatment conditionally on individual characteristics, serves as a key metric for characterizing treatment heterogeneity and identifying units most likely to benefit from treatment [Athey and Imbens, 2016]. Many machine learning models have been developed and applied to estimate CATE using rich sets of features. For example, using electronic health records, Zainal et al. [2024] have found that the causal forest algorithm [Athey et al., 2019] can identify some groups of patients with suicidal ideation who strongly benefit from psychiatric hospitalization, and other groups of patients who may even respond negatively to hospitalization.

One practical limitation of these machine-learning-based approaches is that they usually focus only on understanding, on a unit-by-unit level, who would benefit from receiving a treatment. However, if an organization such as the Veterans Health Administration wanted to operationalize the findings from these approaches, they would also need to consider how the resulting policy might stress their available resources and infrastructure [Hussey et al., 2016]. In the short-to-medium term, the number of available hospital beds is likely a fixed

This research was supported by the Office of Naval Research under grant N00014-24-1-2091.

resource, so beyond a certain point, assigning more patients to inpatient care may cause delays or reduce resource availability for other patients.

The goal of this work is to augment machine-learning-based methods for optimal targeting, such as causal forests, to make them aware of (and responsive to) capacity constraints induced by the system’s dynamics that may stochastically limit or delay the number of units that can receive treatment at any given time. We believe this to be a problem setting with broad applicability. For example, such methods could be used for targeting expedited delivery in online delivery platforms or fast-track care in the emergency department. In order to address long wait times in emergency departments, some hospitals implement fast-track systems to divert patients with more minor illnesses from the main intake system and enable them to get faster care [Meislin et al., 1988]. Using a machine learning system to target assignment to the fast-track system could be promising; however, any such system should also be aware of the current queuing conditions and capacity resources of the hospital.

The problem of optimal treatment assignment in a dynamic system is a reinforcement learning problem—and, when working with complex or high-dimensional inputs as are often encountered with, e.g., electronic health records, one might expect this reinforcement learning problem to be intractably complicated. We find, however, our optimal targeting problem admits a simple and intuitive solution: We show that policymakers can account for treatment-induced congestion effects by combining standard treatment prioritization rules with state-dependent decision thresholds.

More specifically, using the hospital admission setting as a motivating example, let $\tau(x, k)$ represent the direct effect of hospitalization for patients with health records x given the level of system congestion k ; following Munro et al. [2025], we refer to this quantity as Conditional Average Direct Effect (CADE). Then, our results show that the optimal policy must take the form of a CADE-thresholding rule with state-specific thresholds c_k , and assigns treatment only to those whose health records X_i satisfy $\tau(X_i, k) > c_k$. This structure closely mirrors that of optimal treatment prioritization rules under static budget constraints [Bhattacharya and Dupas, 2012, Sun et al., 2021]. The relationship between these thresholds c_k , as well as their magnitude, is shaped by the intricate interplay of the system’s dynamics, the distribution of covariates, and the outcome function, each of which can vary largely depending on the context. Yet, despite this complexity, we show that these threshold values can be estimated from a single observational dataset by combining standard CADE estimation with a state-level value iteration. In doing so, treatment decisions can be fine-tuned to strike a balance between individual benefit and system capacity.

1.1 Related Work

The problem of learning optimal targeting rules has been extensively studied over the past two decades, primarily in settings where treatment assignments are considered independently across units [Manski, 2004, 2009, Hirano and Porter, 2009, Stoye, 2009, 2012, Qian and Murphy, 2011, Kitagawa and Tetenov, 2018, Kallus, 2018, Luedtke and Chambaz, 2020, Athey and Wager, 2021]. Works in this vein have then focused on deriving regret-optimal treatment rules in heterogeneous populations that depend solely on the focal unit’s condition. In such settings, recent advances in machine learning allow accounting for heterogeneous treatment effects based on a rich set of covariates [Chernozhukov et al., 2018, 2022, Athey et al., 2019, Nie and Wager, 2021, Farrell et al., 2021, Kennedy et al., 2024]. Our approach differs from those by also considering the potential interactions between different treatment assignments that arise from a shared pool of limited resources, particularly in the form of

stochastic delay or congestion.

Our work deals with dynamic capacity constraints limiting the number of units eligible for treatment. From this perspective, our research is related to the strand of literature on finding optimal targeting rules under budget constraints [Bhattacharya and Dupas, 2012, Luedtke and van der Laan, 2016, Wang et al., 2018, Le et al., 2019, Huang and Xu, 2020, Sun, 2021, Sun et al., 2021, Xu et al., 2022, Kitagawa and Wang, 2023b, Zhou et al., 2023, Imai and Li, 2023, Sverdrup et al., 2024, Yadlowsky et al., 2025]. However, these works typically assume a fixed, one-time budget—where resources are permanently depleted once allocated—whereas our approach considers dynamic resource capacity, which can recover as units are served and exit the system.

Shared capacity or state can be understood as a form of interference, where the treatment assigned to units arriving earlier may affect the outcomes of units arriving later. While there is a growing body of literature that studies the estimation of treatment effects under interference within the Neyman–Rubin framework [Hudgens and Halloran, 2008, Tchetgen Tchetgen and VanderWeele, 2012, Manski, 2013, Aronow and Samii, 2017, Basse et al., 2019, Sävje et al., 2021, Li and Wager, 2022, Leung, 2022, Farias et al., 2022, Zhan et al., 2024, Johari et al., 2024], including the recent works that study causal inference and experimentation under stochastic congestion [Li et al., 2023, Boutilier et al., 2024], few studies have focused on optimal targeting under such conditions. Existing works in this area tend to address the challenge by determining a single targeting rule for the entire population at once [Galeotti et al., 2020, Ananth, 2020, Kitagawa and Wang, 2023a,b, Zhang and Imai, 2023, Viviano, 2024, Munro et al., 2025], whereas the problem we consider involves sequential targeting, where decisions are made one at a time as units arrive in the system. The targeting threshold in our framework is conceptually related to the conditional average indirect effect studied in Munro et al. [2025], which extends the average indirect effect studied in Hu et al. [2022] and Li and Wager [2022]. However, unlike those works, our method does not require explicitly estimating this effect through augmented experiments with perturbations.

Our work is also closely related to the literature on off-policy learning in dynamic processes. Early contributions in this field primarily focused on learning a sequence of treatment rules that depend on the entire history of the process [Murphy, 2003, 2005, Robins, 2004, Zhang et al., 2013, Nie et al., 2021]. This approach imposes restrictions on both the total number of periods and the complexity of the historical information being tracked. In the average reward setting that we consider [Howard, 1960], a more common approach is to model the system as a Markov decision process [Sutton et al., 1999, Adusumilli et al., 2019, Zhang and Ross, 2021, Kallus and Zhou, 2021]. The conditional average effects we study are closely related to the difference-of-Q formulation introduced in the recent reinforcement learning literature, which captures the impact of policy deviations [Farias et al., 2022, Cao and Zhou, 2024, Johari et al., 2025]. A key distinction between the Markov model we use and those commonly found in the literature is the handling of covariates. We assume that the units’ covariates are exogenous, which allows us to separate individual-level characteristics tied to a unit’s own treatment experience from the system-level state that passes down through the system and affects future units. In contrast, typical MDP models often blur the distinction between individual covariates and system states, thus leading to complex dynamics and inflated policy spaces.

A particularly relevant line of work studies structured Markov decision processes motivated by operational systems and exogenous inputs. One related strand studies mixed systems in queuing-motivated settings, where the state is decomposed into a stochastic component and a pseudo-stochastic component whose update rule is known, which enables

virtual sample generation [Wei et al., 2023]. A separate strand studies exogenous MDP formulations, where the decision maker can exploit known or partially known structure in the endogenous dynamics and rewards while learning the effect of exogenous randomness [Dietterich et al., 2018, Efroni et al., 2022, Kallus and Zhou, 2022, Sinclair et al., 2023, Wan et al., 2024]. These models are related to ours in separating exogenous inputs from endogenous system states, but differ in their statistical focus: in our setting, both the reward function and the state-transition mechanism are unknown and must be learned from data.

Finally, at a higher level, the problem we aim to address is closely related to those studied in the dynamic resource allocation and optimal control literature [e.g., Naor, 1969, Johansen and Stidham Jr, 1980, Chen and Frank, 2001, Borgs et al., 2014, Xu and Chan, 2016, Agrawal and Jia, 2019, Cheung and Simchi-Levi, 2019, Murthy et al., 2022, Chen et al., 2024, Boutilier et al., 2024, and references therein]. Much of this literature has focused on managing limited capacity with system-level objectives and often abstracts away individual-level heterogeneity. More recently, there has been a growing interest in data-driven approaches that leverage covariate or contextual information to improve decision-making in revenue and inventory management [Feng and Shanthikumar, 2018, Ban and Rudin, 2019, Bertsimas and Kallus, 2020, Chen et al., 2022, Ding et al., 2024], as well as in patient prioritization and triage [Jacobson et al., 2012, Mills et al., 2013, Shi et al., 2024, Keskin and Zhang, 2024, Bansak et al., 2024]. Our work contributes to this literature by introducing a perspective that bridges causal machine learning tools with dynamic constraints, which enables simple, interpretable decision making even in the presence of complex covariates.

2 Targeting in Dynamic Systems

Consider the problem of targeting in a single dynamic system, where units $i = 1, \dots, n$ arrive sequentially. When each unit i arrives, we observe their covariate $X_i \in \mathcal{X}$ and decide on a treatment $W_i \in \{0, 1\}$ to assign. Each time a unit arrives and is assigned a treatment, this may alter the system’s dynamics. We capture this dynamic feature using the state variable $S_i \in \mathcal{S}$, which represents the system’s condition at the time of the unit’s arrival. The unit’s outcome, $Y_i \in \mathbb{R}$, may depend on their covariate X_i , the treatment assignment W_i , and the current state S_i . Let $\pi : \mathcal{X} \times \mathcal{S} \rightarrow [0, 1]$ denote the treatment assignment policy, i.e., $\mathbb{P}[W_i = 1 \mid X_i = x, S_i = s] = \pi(x, s)$ under policy π . We use the outcome as a proxy for utility and are interested in learning a good policy π from an observed dataset of size n that maximizes the average outcome.

Example 1 (Emergency Department Triage). In a hospital emergency department, patients arrive sequentially, each with observed clinical features X_i . The hospital needs to decide whether to offer fast-track treatment ($W_i = 1$) or place the patient in the regular queue ($W_i = 0$). The system state S_i reflects the numbers of patients currently in each queue. The patient’s health outcome may depend on both their clinical features and the queue length of the queue they are assigned to.

Example 2 (Routing Customer Support Requests). In an online service platform, customer support tickets arrive sequentially, each with observed features X_i such as account information and request details. The platform decides whether to route the ticket to a specialist ($W_i = 1$) or assign it to regular support staff which is not capacity-constrained ($W_i = 0$). The system state S_i represents the number of unresolved tickets awaiting specialist attention. The customer’s satisfaction score may depend on the assignment, their features, and specialist queue length if routed to them.

One common targeting strategy is to estimate the Conditional Average Treatment Effect (CATE) from a sample of n units, and implement a policy that targets all units with a positive estimated CATE [Manski, 2004, Stoye, 2012, Tetenov, 2012]. In our dynamic setting, the natural state-aware analogue of the CATE is

$$\tau(x, s) := \mathbb{E} [Y_i \mid X_i = x, S_i = s, W_i = 1] - \mathbb{E} [Y_i \mid X_i = x, S_i = s, W_i = 0]. \quad (1)$$

However, as we will discuss later, this quantity only captures the direct effect of the treatment on the current individual, and misses its potential impact on later individuals through changes in the system state. Thus, in what follows, we refer to $\tau(x, s)$ as the Conditional Average Direct Effect (CADE), and refer to the CADE-based targeting strategy as the direct targeting rule.

Definition 1 (Direct Targeting Rule). Let $\hat{\tau}(x, s)$ be an estimated CADE from the dataset. The direct targeting rule π^d assigns treatment whenever $\hat{\tau}(x, s) > 0$, i.e., $\pi^d(x, s) = I(\hat{\tau}(x, s) > 0)$.

One might think that this targeting strategy already accounts for the dynamic nature of the system, since the state variable S_i is also used for targeting. For example, if the treatment represents admission to a system and the state variable represents the busyness level of the system, the direct targeting rule might only assign individuals to the system when it is not busy. However, this argument overlooks how the treatment assignment might affect the system state. Under a direct targeting rule, individuals who benefit only marginally from treatment may still join the system, potentially causing congestion that crowds out individuals for whom treatment would have had substantial benefit. In fact, as we will show later, the direct targeting rule may only be optimal when the treatment assignment has little impact on state evolution, or when all units are insensitive to the system’s state.

We first make the following assumptions about the stability of the system, which allow us to formally define an optimal policy in a dynamic system.

Assumption 1 (Time-Homogeneous MDP with Exogenous Covariates). The system transition is governed by a set of time-homogeneous distributions $\{P_X(\cdot), P_Y(\cdot \mid x, s, w), P_S(\cdot \mid s, w)\}$ such that, for all units i and conditionally on the past, X_i, Y_i and S_{i+1} are drawn according to the densities $P_X(\cdot), P_Y(\cdot \mid X_i, S_i, W_i)$ and $P_S(\cdot \mid S_i, W_i)$.

Assumption 2 (Irreducibility and Boundedness). The process $\{S_i \mid i = 1, 2, \dots\}$ induced by any policy π is irreducible and aperiodic. Furthermore, the state space \mathcal{S} is finite, and the outcomes Y_i are almost surely uniformly bounded by a constant M_Y .

A representation of such a Markov decision process with exogenous covariates can be found in Figure 1. In Section A, we provide a concrete example of how this framework naturally models queuing admission and routing systems, and discuss how similar ideas can extend to related dynamic resource-allocation settings.

Assumptions 1 and 2 ensure that there exists a unique stationary distribution of the state (denoted as d_π), and the average outcome under the policy π exists and can be reduced to the following form that does not rely on the initial state:

$$\lim_{n \rightarrow \infty} \mathbb{E} \left[\frac{1}{n} \sum_{i=1}^n Y_i \mid S_1 = s \right] = \mathbb{E}_\pi [Y_i] =: \mu(\pi), \quad (2)$$

where the expectation is taken over the joint distribution of P_Y, P_X , and the stationary distribution d_π , i.e., $\mathbb{E}_\pi [Y_i] = \int_{\mathcal{X}} \sum_{s \in \mathcal{S}} P_X(x) d_\pi(s) \mathbb{E}_\pi [Y_i \mid S_i = s, X_i = x] dx$ [Van Roy, 1998]. We say that a policy is optimal if it maximizes the average outcome $\mu(\pi)$.

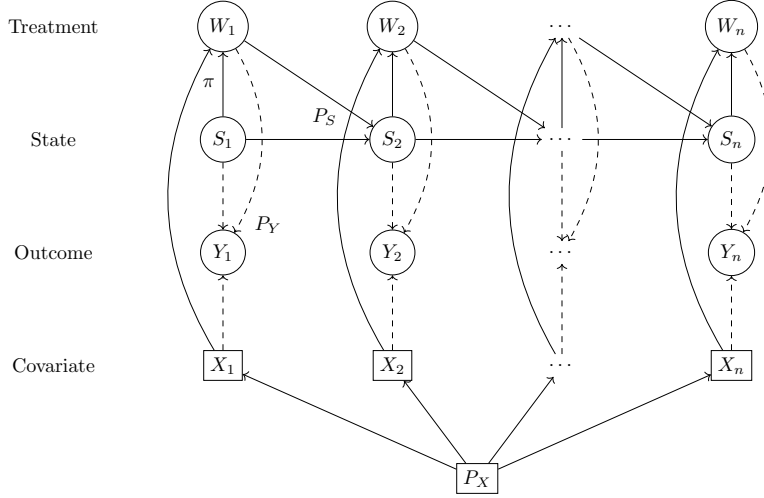


Figure 1: An illustration of a sample of size n drawn from a time-homogeneous Markov decision process with exogenous covariates.

Definition 2 (Optimal Targeting Rule). A targeting rule $\pi^* : \mathcal{X} \times \mathcal{S} \rightarrow [0, 1]$ is optimal if

$$\pi^* \in \arg \max_{\pi} \mu(\pi). \quad (3)$$

2.1 A Threshold Characterization with Dynamic Shadow Costs

A direct targeting rule assigns treatment whenever the current unit's estimated CADE is positive. In a dynamic system, however, this comparison is incomplete. Assigning treatment to the current unit can change the future state of the system, and thus affect the outcomes of later units. This raises the question of how the usual direct targeting rule should be adjusted to account for this downstream impact. In this section, we show that the adjustment takes a simple form: the optimal policy compares the CADE to a state-specific threshold c_s , where c_s represents the dynamic shadow cost of assigning treatment when the system is in state s . We first derive this threshold form from the state-level Bellman equation induced by the exogenous-covariate structure, and then connect the characterization to a direct/indirect effect decomposition, where the CADE captures only the direct component of the marginal value of treatment, while our state-specific threshold captures the negative indirect component induced by downstream changes in the system.

For notational convenience, write

$$\eta_w(x, s) := \mathbb{E} [Y \mid X = x, S = s, W = w], \quad P_{S,w}(s'|s) := P_S(s'|s, w) \quad (4)$$

for the conditional average outcome and the state transition kernel under treatment $w \in \{0, 1\}$. Recall that $\tau(x, s) = \eta_1(x, s) - \eta_0(x, s)$, and write $\mu^* := \sup_{\pi} \mu(\pi)$ for the optimal long-run average outcome. Under the exogenous-covariate structure in Assumption 1, the continuation value of a policy depends only on the system state s , rather than on the full covariate-state pair (x, s) . After integrating over the exogenous covariate distribution, the dynamic component of the problem can therefore be viewed as a finite-state average-reward dynamic program on \mathcal{S} . The standard average-reward Bellman equation for this reduced problem [e.g., Puterman, 1994] then yields the following state-level characterization.

Lemma 1. *Under Assumptions 1 and 2, there exists a relative value function $V^* : \mathcal{S} \rightarrow \mathbb{R}$ such that*

$$\mu^* + V^*(s) = \mathbb{E}_X \left[\max_{w \in \{0,1\}} \eta_w(X, s) + \sum_{s' \in \mathcal{S}} P_{S,w}(s'|s) V^*(s') \right], \quad s \in \mathcal{S}. \quad (5)$$

Moreover, any deterministic policy π^* that satisfies

$$\pi^*(x, s) \in \operatorname{argmax}_{w \in \{0,1\}} \left\{ \eta_w(X, s) + \sum_{s' \in \mathcal{S}} P_{S,w}(s'|s) V^*(s') \right\} \quad (6)$$

for all $(x, s) \in \mathcal{X} \times \mathcal{S}$ is optimal.

The key feature of the state-level Bellman equation in Lemma 1 is that the relative value function depends only on the state s but not directly on the covariate x . Below, we show that this separation leads to a particularly simple characterization of the optimal policy. Within each state, the policy compares the CADE to a state-specific continuation-value adjustment. Thus, the optimal rule keeps the familiar CADE ranking of the direct targeting rule within each state, but shifts the treatment cutoff according to the continuation-value impact of using capacity in that state.

Theorem 2. *Under Assumptions 1 and 2, there exists an optimal deterministic policy of the form*

$$\pi^*(x, s) = I(\tau(x, s) > c_s), \quad (7)$$

where $c_s = -\sum_{s' \in \mathcal{S}} (P_{S,1}(s'|s) - P_{S,0}(s'|s)) V^*(s')$.

The threshold c_s can be understood as the dynamic shadow cost of assigning treatment in state s . Consider the normalized policy gradient at a given covariate-state pair,¹

$$H(x, s; \pi) = \frac{1}{P_X(x) \cdot d_\pi(s)} \frac{\partial}{\partial \pi(x, s)} \mu(\pi), \quad (8)$$

which represents the marginal value of increasing the treatment assignment probability for units with covariate $X_i = x$ who arrive when the system is in state $S_i = s$. By the average-reward policy-gradient theorem [Marbach and Tsitsiklis, 2001], $H(x, s; \pi)$ can be decomposed into the CADE and a Conditional Average Indirect Effect (CAIE):

$$H(x, s; \pi) = \underbrace{\tau(x, s)}_{\text{CADE}} + \underbrace{C_\pi(s)}_{\text{CAIE}}, \quad (9)$$

where the CAIE

$$C_\pi(s) = \lim_{n \rightarrow \infty} \mathbb{E}_\pi \left[\sum_{i=2}^n (Y_i - \mu(\pi)) \mid S_1 = s, W_1 = 1 \right] - \lim_{n \rightarrow \infty} \mathbb{E}_\pi \left[\sum_{i=2}^n (Y_i - \mu(\pi)) \mid S_1 = s, W_1 = 0 \right]$$

captures the downstream marginal impact of treatment through future changes in the system state. Under an optimal policy, $c_s = -C_{\pi^*}(s)$. In other words, c_s is the state-specific

¹We divide the policy gradient by $P_X(x) \cdot d_\pi(s)$, the probability of observing the covariate-state pair (x, s) , to isolate the conditional impact of adjusting the policy for units with covariate x in state s .

dynamic shadow cost of assigning treatment in state s at optimum. For example, in a queuing system, Theorem 2 suggests that the optimal policy should apply a different treatment threshold at each queue length, and this threshold captures the expected cumulative impact on future outcomes from admitting one additional patient at that queue length under the optimal policy.

We note that our state-aware CADE thresholding approach strictly generalizes the standard direct targeting rule in Definition 1. In the classical setting where the treatment does not affect the system’s dynamics, the indirect effect $C_\pi(s)$ is always zero.² Thus, the optimal policy is simply to compare the CADE with zero, resulting in the direct targeting rule $\pi^*(x, s) = I(\tau(x, s) > 0)$.

2.2 A State-Aware CADE Thresholding Algorithm

Theorem 2 suggests that the dynamic targeting problem can be solved by augmenting direct targeting with a state-dependent continuation-value adjustment:

1. Estimate $\hat{\tau}(x, s)$ via a standard causal machine learning method, such as a causal forest [Athey et al., 2019] or an X -learner [Künzel et al., 2019].
2. Estimate a state-level relative value function V^* by applying relative value iteration [Puterman, 1994] to the empirical Bellman optimality equation, and recover the state-specific treatment thresholds c_s .

Writing $r_0(s) := \mathbb{E}_X [\eta_0(X, s)]$ for the expected reward under treatment $W_i = 0$ at state s , the state-level Bellman operator can be expressed as

$$\begin{aligned} (T_S v)(s) &:= \mathbb{E}_X \left[\max_{w \in \{0,1\}} \eta_w(X, s) + \sum_{s' \in \mathcal{S}} P_{S,w}(s'|s)v(s') \right] \\ &= r_0(s) + (P_{S,0}v)(s) + \mathbb{E}_X \left[(\tau(X, s) + ((P_{S,1} - P_{S,0})v)(s))_+ \right]. \end{aligned} \quad (10)$$

Thus, the Bellman recursion remains state-level, where the covariates enter through the CADE while the continuation-value recursion is defined only on the state space \mathcal{S} .

To form an empirical version of the Bellman operator T_S , we split the trajectory into a training sample \mathcal{I}_t and an evaluation sample \mathcal{I}_e . On the training sample, we obtain estimates of the CADE, $\hat{\tau}(x, s)$, and of the transition kernels, $\hat{P}_{S,w}(s'|s)$, $w \in \{0,1\}$. The CADE estimate can be obtained using any suitable conditional treatment effect learner, and the transition kernels can be estimated by empirical conditional transition frequencies

$$\hat{P}_{S,w}(s'|s) = \frac{\sum_{i \in \mathcal{I}_t} I(S_i = s, W_i = w, S_{i+1} = s')}{\sum_{i \in \mathcal{I}_t} I(S_i = s, W_i = w)}. \quad (11)$$

Using the training sample, we also obtain estimates of the conditional outcome $\eta_0(x, s)$ and the behavior policy $\pi_0(x, s) := \mathbb{P}[W_i = 1 | X_i = x, S_i = s]$,³ denoted by $\hat{\eta}_0(x, s)$ and $\hat{\pi}_0(x, s)$, for estimating the average baseline outcome $r_0(s)$.

²This phenomenon, i.e., that the average direct effect of a treatment in a system with spillovers matches the average treatment effect in a system where spillovers are suppressed, has also been observed in many different models [e.g., Sävje et al., 2021, Munro et al., 2025].

³We implicitly assume that the status-quo policy depends only on (X_i, S_i) . This assumption, often referred to as sequential ignorability [Hernán and Robins, 2020, Wager, 2025], is reasonable in our context, as treatment decisions are typically made based on features observable to the system at the time of arrival.

Algorithm 1 State-Aware CADE Thresholding (SACT) by Relative Value Iteration

- 1: **Data:** (X_i, S_i, W_i, Y_i) , $i = 1, \dots, n$
- 2: Split the data into a training sample \mathcal{I}_t and an evaluation sample \mathcal{I}_e
- 3: On the training sample \mathcal{I}_t , estimate $\hat{\tau}(x, s)$, $\hat{P}_{S,w}(s' | s)$, $w = 0, 1$, and the nuisance functions $\hat{\eta}_0(x, s)$ and $\hat{\pi}_0(x, s)$
- 4: Using \mathcal{I}_e , construct $\hat{r}_0(s)$ and the empirical Bellman operator \hat{T}_S as in (12) and (13)
- 5: Initialize a value function $V^{(0)} : \mathcal{S} \rightarrow \mathbb{R}$ and choose an anchor state s_0
- 6: **for** $m = 0, 1, 2, \dots$ until convergence **do**
- 7: Given $V^{(m)}$, compute $\tilde{V}^{(m+1)}(s) = (\hat{T}_S V^{(m)})(s)$ for all $s \in \mathcal{S}$
- 8: Recenter with $V^{(m+1)}(s) = \tilde{V}^{(m+1)}(s) - \tilde{V}^{(m+1)}(s_0)$, $s \in \mathcal{S}$, so that $V^{(m+1)}(s_0) = 0$
- 9: **end for**
- 10: **Output:** Set $\hat{V}^* := V^{(m+1)}$ and output

$$\hat{\pi}(x, s) = I \left(\hat{\tau}(x, s) > - \sum_{s' \in \mathcal{S}} \{ \hat{P}_{S,1}(s' | s) - \hat{P}_{S,0}(s' | s) \} \hat{V}^*(s') \right)$$

Conditional on these estimates, the evaluation sample is then used both to estimate the average baseline outcome and to approximate the expectation over X in the state-level Bellman operator. Let $\mathcal{I}_e(s) = \{i \in \mathcal{I}_e : S_i = s\}$. We first estimate $r_0(s)$ through the doubly robust estimator

$$\hat{r}_0(s) := \frac{1}{|\mathcal{I}_e(s)|} \sum_{i \in \mathcal{I}_e(s)} \left[\hat{\eta}_0(X_i, s) + \frac{I(W_i = 0)}{1 - \hat{\pi}_0(X_i, s)} \{Y_i - \hat{\eta}_0(X_i, s)\} \right] \quad (12)$$

using the nuisance components $\hat{\eta}_0(x, s)$ and $\hat{\pi}_0(x, s)$ estimated on the training sample, and then form the empirical state-level Bellman operator

$$(\hat{T}_S v)(s) := \hat{r}_0(s) + \left(\hat{P}_{S,0} v \right)(s) + \frac{1}{|\mathcal{I}_e|} \sum_{i \in \mathcal{I}_e} \left(\hat{\tau}(X_i, s) + \left((\hat{P}_{S,1} - \hat{P}_{S,0}) v \right)(s) \right)_+ \quad (13)$$

We summarize our proposed approach to targeting in dynamic systems based on this empirical state-level Bellman operator in Algorithm 1.

Given a current estimate of the continuation value, Algorithm 1 selects the treatment action that maximizes the estimated one-step reward plus continuation value, and then recenters the resulting value function. Running Algorithm 1 requires splitting the sample into a training and evaluation set. This sample-splitting step may initially appear to be less straightforward, as the data points are correlated due to the system's dynamics. However, for each fixed state $s \in \mathcal{S}$, the system regenerates whenever it returns to state s , and the data becomes independent of the preceding trajectory after each regeneration [Ross, 2014]. Therefore, we can split the dataset by first dividing the trajectory into i.i.d. chunks based on occurrences of a chosen state s , and then randomly assigning these chunks to the training or evaluation set. In practice, one can choose a frequently visited state s to obtain more balanced regenerative blocks, and use these blocks to implement cross-fitting rather than relying on a single training/evaluation split.

Remark 1. When the behavior policy π_0 is known, the baseline reward $r_0(s)$ can instead be

estimated directly by the inverse-probability-weighted estimator

$$\hat{r}_0^{\text{IPW}}(s) := \frac{1}{|\{i : S_i = s\}|} \sum_{i: S_i = s} \frac{I(W_i = 0)}{1 - \pi_0(X_i, s)} Y_i. \quad (14)$$

The doubly robust form in (12) is used to accommodate the more general setting where the behavior policy is unknown and may need to be estimated, possibly with high-dimensional covariates. In this case, directly plugging in $\hat{\pi}_0$ in the IPW estimator can introduce first-order sensitivity to behavior-policy estimation error. The augmentation by the baseline outcome regression $\hat{\eta}_0$ removes this first-order sensitivity, so that the remaining nuisance bias is of the usual product form.

2.3 Statistical Guarantees

We next provide some generic upper bounds—under abstract high-level conditions—on the regret attained by our proposed procedure. For a stationary policy $\pi : \mathcal{X} \times \mathcal{S} \rightarrow \{0, 1\}$, define

$$P_{S, \pi}(s' | s) := \mathbb{E}_X [\pi(X, s) P_{S, 1}(s' | s) + (1 - \pi(X, s)) P_{S, 0}(s' | s)], \quad (15)$$

and similarly

$$\hat{P}_{S, \pi}(s' | s) := \frac{1}{|\mathcal{I}_e|} \sum_{i \in \mathcal{I}_e} \left(\pi(X_i, s) \hat{P}_{S, 1}(s' | s) + (1 - \pi(X_i, s)) \hat{P}_{S, 0}(s' | s) \right). \quad (16)$$

We impose the following uniform mixing assumption on both the true and the empirical transition kernels.

Assumption 3 (Uniform Mixing). There exist constants $t_0 \geq 0$ and $t_{\text{mix}} \geq 1$ such that, for all $t \geq t_0$ and every stationary policy π , the kernels $P_{S, \pi}$ and $\hat{P}_{S, \pi}$ admit unique stationary distribution d_π and $d_{\hat{P}, \pi}$, and

$$\sup_{s \in \mathcal{S}} |P_{S, \pi}^t(\cdot | s) - d_\pi|_{\text{TV}} \leq e^{-t/t_{\text{mix}}}, \quad \sup_{s \in \mathcal{S}} |\hat{P}_{S, \pi}^t(\cdot | s) - d_{\hat{P}, \pi}|_{\text{TV}} \leq e^{-t/t_{\text{mix}}}. \quad (17)$$

Under Assumptions 1-2, the true kernel $P_{S, \pi}$ is induced by a finite-state irreducible and aperiodic Markov chain, and hence such a finite mixing time always exists. By contrast, the empirical kernel $\hat{P}_{S, \pi}$ may not automatically inherit these properties. In practice, an anchored version of $\hat{P}_{S, \pi}$ can often be used to ensure that the above mixing assumption is satisfied by mixing $\hat{P}_{S, \pi}$ with a fixed reference kernel; see, for example, Zurek and Chen [2024].

Lemma 3. *Suppose Assumptions 1-3 hold. Then,*

$$\begin{aligned} \left\| \hat{V}^* - V^* \right\|_\infty &\lesssim (t_0 + t_{\text{mix}}) \left(\|\hat{r}_0 - r_0\|_\infty + \max_{s \in \mathcal{S}} \|\hat{\tau}(\cdot, s) - \tau(\cdot, s)\|_{L_2(P_X)} \right) \\ &\quad + M_Y (t_0 + t_{\text{mix}})^2 \max_{w \in \{0, 1\}} \left\| \hat{P}_{S, w} - P_{S, w} \right\|_{\infty, 1} + \mathcal{O}_P \left(|\mathcal{I}_e|^{-1/2} \right). \end{aligned} \quad (18)$$

where $\left\| \hat{P}_{S, w} - P_{S, w} \right\|_{\infty, 1} := \max_{s \in \mathcal{S}} \sum_{s' \in \mathcal{S}} \left| \hat{P}_{S, w}(s' | s) - P_{S, w}(s' | s) \right|$.

Lemma 3 shows how estimation error propagates through the dynamic system under the exogenous-covariate formulation. Errors in estimating the baseline reward and the CADE create local Bellman errors whose impact accumulates over future periods at a rate proportional to the mixing time. By contrast, errors in estimating the transition kernels enter through the continuation-value term and are therefore amplified by both the mixing time and the size of the downstream value function, which leads to the stronger t_{mix}^2 dependence. This decomposition is reminiscent of the simulation lemma for discounted MDPs [Kearns and Singh, 2002, Agarwal et al., 2026], in which estimation error in the immediate reward component propagates through the system linearly in the stability factor, whereas transition-kernel error is amplified by an additional factor because it acts through the downstream value function.

In particular, the potentially complex covariate X affects the bound only through estimation of the CADE $\tau(x, s)$ and does not enter recursively through a value function on the full (X, S) space. This separation is especially helpful because CADE estimation can often be handled with modern doubly robust or orthogonal methods, whereas the dynamic burden is confined to the much smaller state-level transition object. In Section 2.4, we discuss how this separation can substantially reduce the statistical complexity of standard plug-in policy-learning methods in a tabular setting.

Before stating the regret bound, we impose a standard nuisance condition for the doubly robust baseline reward estimator $\hat{r}_0(s)$. This condition requires overlap for the behavior policy and the usual product-rate control for the nuisance estimates. The additional boundedness requirements on the estimated nuisance functions are technical stability conditions, and can be enforced in practice by truncating $\hat{\pi}_0$ away from zero and one and clipping $\hat{\eta}_0$ to the bounded outcome range.

Assumption 4 (Overlap and Nuisance Regularity). The behavior policy satisfies the overlap condition that there exists a constant $\Gamma_1 > 0$ such that $\Gamma_1 \leq \pi_0(x, s) \leq 1 - \Gamma_1$ for all $(x, s) \in \mathcal{X} \times \mathcal{S}$. The nuisance estimates $\hat{\eta}_0(x, s)$ and $\hat{\pi}_0(x, s)$ satisfy

$$\max_{s \in \mathcal{S}} \|\hat{\eta}_0(X_i, s) - \eta_0(X_i, s)\|_{L_2(P_X)} \cdot \|\hat{\pi}_0(X_i, s) - \pi_0(X_i, s)\|_{L_2(P_X)} = \mathcal{O}_p\left(\frac{1}{\sqrt{n}}\right). \quad (19)$$

Moreover, $\hat{\pi}_0(x, s)$ is bounded away from zero and one and $\hat{\eta}_0(x, s)$ is uniformly bounded almost surely for all (x, s) .

Theorem 4. Under Assumptions 1-4, if $\hat{\tau}(x, s)$ learned on the training set \mathcal{I}_t satisfies

$$\max_{s \in \mathcal{S}} \|\hat{\tau}(X_i, s) - \tau(X_i, s)\|_{L_2(P_X)} = \mathcal{O}_p\left(|\mathcal{I}_t|^{-\beta}\right), \quad \beta > 0, \quad (20)$$

then the policy $\hat{\pi}$ generated by Algorithm 1 with $|\mathcal{I}_t|, |\mathcal{I}_e| \asymp n$ satisfies

$$\mu(\pi^*) - \mu(\hat{\pi}) = \mathcal{O}_P\left(n^{-(\beta \wedge \frac{1}{2})}\right). \quad (21)$$

Theorem 4 shows that augmenting the direct CADE-thresholding rule with state-aware thresholds yields regret of order $\mathcal{O}_P(n^{-(\beta \wedge \frac{1}{2})})$. In flexible nonparametric settings, the CADE estimation rate is typically no faster than the parametric rate, so the leading term in this bound is often the error in estimating $\tau(x, s)$. In this sense, our result has the same qualitative flavor as plug-in thresholding results in the i.i.d. setting, where a basic bound controls

regret by the error in estimating the conditional effect, while sharper plug-in rates typically require additional margin assumptions controlling the amount of covariate mass near the decision boundary [Luedtke and Chambaz, 2020]. In our setting, the analogous margin condition would control the amount of covariate mass near the state-specific decision boundaries $\tau(x, s) = c_s$, but we do not impose such conditions here. We also note that our assumed uniform $L_2(P_X)$ -norm bound on the estimated CADE function $\hat{\tau}(X_i, s)$ over states $s \in \mathcal{S}$, i.e., (20), can be attained when the state space \mathcal{S} is finite (as in Assumption 2) by leveraging a large body of literature on non-parametric CATE estimation [see, e.g., Kennedy, 2023, for a discussion].⁴

2.4 Comparison with the General Collapsed-State Approach

A key idea of our approach has been our ability to separate individual characteristics from the system state: We assume that the characteristics X capture heterogeneity in the current unit’s outcomes, while the dynamic consequences of current decisions are carried forward by a lower-dimensional system state S . This separation allows the Bellman recursion in Section 2.2 to remain lower dimensional. To elucidate the value of this structure, it is natural to ask what would happen if instead we ran an algorithm that ignores this separation and treated the pair (X, S) as a single Markov state, as one would if tackling our problem with off-the-shelf reinforcement learning tools. Does our proposed approach out-perform such an off-the-shelf baseline—and, if yes, by how much?

When the covariate and the system state are collapsed into a single Markov state, $Z := (X, S) \in \mathcal{X} \times \mathcal{S}$, the problem becomes a standard Markov decision process with state variable Z , and the corresponding Bellman operator takes the form

$$(Tv)(z) := \max_{w \in \{0,1\}} \left(\eta_w(z) + \sum_{z' \in \mathcal{X} \times \mathcal{S}} P_{Z,w}(z' | z)v(z') \right), \quad (22)$$

For simplicity, we here focus the tabular setting where both \mathcal{X} and \mathcal{S} are finite, so relevant model primitives can be estimated by plug-in sample averages. This enables us to compare our proposed method to standard methods for tabular MDPs [e.g., Kearns and Singh, 2002], which provide a direct benchmark for assessing the statistical benefit of treating (X, S) as a generic Markov state rather than exploiting the exogenous-covariate structure.

For our proposed method, we form a plug-in version of the state-level operator (10) by estimating $\tau(x, s)$, $r_0(s)$, the covariate distribution P_X , and the state-level transition kernels $P_{S,w}(\cdot | s)$ via tabular averaging from the data, and then applying relative value iteration on the state space \mathcal{S} . For the collapsed-state baseline, we instead estimate the reward functions $\eta_w(z)$ and the collapsed transition kernels $P_{Z,w}(\cdot | z)$ on the full state space $\mathcal{X} \times \mathcal{S}$, and apply relative value iteration to the Bellman operator (22). The following result provides regret bounds for both approaches via the same standard proof technique, i.e., by using concentration bounds for plug-in estimates to control the Bellman-operator error and then propagating this error through the Bellman equation, as in standard simulation-lemma analyses of model-based MDPs [Agarwal et al., 2026].

⁴One potential concern is that the units in our setting are correlated, and thus theories developed for CATE estimation in i.i.d. settings may not directly apply. However, we note that it is possible to construct a subset of the data with size $\mathcal{O}_p(n)$ by randomly selecting a single data point from each i.i.d. chunk, formed based on occurrences of some fixed chosen state s . This approach allows us to retain i.i.d.-like properties, so we still expect the same convergence rate to hold.

Proposition 5. *Under Assumptions 1-4, suppose in addition that \mathcal{X} is finite and that there exists a constant $\Gamma_2 > 0$ such that, for all $(x, s) \in \mathcal{X} \times \mathcal{S}$,*

$$P_X(x) d_{\pi_0}(s) \geq \frac{\Gamma_2}{|\mathcal{X}||\mathcal{S}|}. \quad (23)$$

Then, our method $\hat{\pi}$ and the collapsed-state baseline $\hat{\pi}^{col}$ have regret bounded as

$$\begin{aligned} \sqrt{n} (\mu(\pi^*) - \mu(\hat{\pi}^{col})) &= \mathcal{O}_p \left((t_0 + t_{mix})^2 |\mathcal{X}||\mathcal{S}| \sqrt{\log(|\mathcal{X}||\mathcal{S}|)} \right), \\ \sqrt{n} (\mu(\pi^*) - \mu(\hat{\pi})) &= \mathcal{O}_P \left((t_0 + t_{mix}) \sqrt{|\mathcal{X}||\mathcal{S}| \log(|\mathcal{X}||\mathcal{S}|)} + (t_0 + t_{mix})^2 |\mathcal{S}| \sqrt{\log(|\mathcal{S}|)} \right). \end{aligned} \quad (24)$$

Comparing the scaled regret terms on the right-hand-side of (24) we see that $\hat{\pi}$, i.e., the tabular version of our proposed method that separates exogenous covariates from system state, outperforms the collapsed-state baseline by an order of magnitude. Relative to the baseline (and ignoring log factors), the regret bound for $\hat{\pi}$ is reduced by a factor of $\min\{(t_0 + t_{mix}) \sqrt{|\mathcal{X}||\mathcal{S}|}, |\mathcal{X}|\}$. This highlights how, when the covariate space $|\mathcal{X}|$ is even moderately large, our approach is able to achieve considerably stronger guarantees by exploiting the model structure.

Now, of course, Proposition 5 doesn't give a full picture on the relative merits of our approach relative to collapsed-state baselines. First, the result only compares regret upper bounds to each other—although we do emphasize that the upper bounds were derived using the same (standard) technique of plug-in Bellman-operator perturbation. Second, this result only compares various implementations of tabular value iteration. A full analysis of minimax regret performance for optimal targeting in our model with exogenous covariates would be of considerable interest, but is beyond the scope of this paper. In our numerical experiments, we will also compare our approach to different collapsed-state reinforcement learning algorithms, and find that our approach outperforms these baselines in experiments.

3 State-Dependent Arrivals

So far, we have treated the process as indexed by arriving decision units and evaluated a policy by the average outcome per observed unit. This objective is natural when the arrival process is exogenous to the system state and the targeting policy. In some systems, however, the policy can affect not only the outcomes of individuals who enter the system, but also the frequency with which such individuals arrive. For example, users may choose to leave or avoid a digital platform if they anticipate long waiting times. Consequently, the objective may shift from maximizing the average outcome per unit to optimizing the overall benefit accumulated over a fixed time period, such as daily revenue.

To accommodate this setting, we consider an event-level representation that records the timing of events in calendar time. For concreteness, suppose the system is an $M_n/M/1$ queue with state-dependent arrivals. In an $M_n/M/1$ queue, units arrive at rate λ_k when the current queue length is k , and service completions occur at rate μ . We observe a sequence of events $\{\mathbf{E}_i\}_{i=1, \dots, N(T)}$ occurring at times $0 < T_1 < T_2 < \dots < T_{N(T)} < T$, where $N(t) = \max\{i : T_i \leq t\}$ counts the number of events up to time t . Each event is either an arrival, denoted by $A_i = 1$, or a service completion, denoted by $A_i = 0$.

If event i is an arrival, we observe the individual's covariates $X_i \in \mathcal{X}$ and the current queue length $K_i = 0, 1, \dots, \bar{k}$, assign a treatment $W_i \sim \pi(X_i, K_i)$ indicating whether to admit the individual into the queue, and record the reward R_i . If event i is a service completion, no treatment decision is made, and we set $X_i = \emptyset$, $W_i = 2$, and $R_i = 0$ for bookkeeping. Let $\Delta_i := T_i - T_{i-1}$ denote the inter-event time. Since both the arrival rate and the event type depend on the current queue length, Δ_i is generally correlated with K_i .

To summarize, we write $\mathbf{E}_i = (X_i, K_i, A_i, W_i, \Delta_i, R_i)$, where X_i is the incoming unit's condition, A_i is the event type, K_i is the queue length at time T_i , Δ_i is the inter-event time, W_i is the treatment assigned to the incoming unit, and R_i is the unit's outcome. This event-level representation has the same Markov structure as the model in Section 2. In particular, for any fixed scalar outcome constructed from (R_i, Δ_i) , such as the transformed outcome introduced below, the state-aware Bellman characterization can be applied with state $S_i = (K_i, A_i)$.

The framework in Section 2 optimizes an average outcome over the indexed process. In the present setting, however, one may instead be interested in maximizing the long-run reward rate

$$\theta(\pi) = \mathbb{E}_\pi \left[\lim_{T \rightarrow \infty} \frac{1}{T} \sum_{i=1}^{N(T)} R_i \right]. \quad (25)$$

In other words, $\theta(\pi)$ measures the average reward the system achieves per unit of time in the long run. Such average-reward-per-unit-time objectives are commonly studied in Markov renewal and semi-Markov decision processes because they account for the policy-dependent frequency with which rewards are realized [Puterman, 1994, Ross, 2014]. When arrivals are exogenous and occur at a policy-independent rate, maximizing the average reward per arrival is equivalent to maximizing the reward rate. When the arrival rate varies with congestion, however, the two objectives can differ. For example, if the treatment is in terms of healthcare delivery, one would optimize $\mu(\pi)$ if the goal is to improve health outcomes on average for every patient that arrives at the hospital. On the other hand, one would optimize $\theta(\pi)$ if the goal is to maximize the total benefit (e.g., the overall amount of health improvement) obtained within a fixed amount of time.

A standard result for Markov renewal processes (see, e.g., Chapter 7 of Ross [2014]) implies that, for any fixed policy π , the long-run reward rate can be written as

$$\theta(\pi) = \mathbb{E}_\pi [R_i] / \mathbb{E}_\pi [\Delta_i], \quad (26)$$

where the expectations are taken under the stationary distribution of the event-level process induced by π . In other words, the long-run reward rate can be written as the ratio of the average reward per unit, $\mathbb{E}_\pi [R_i]$, to the average inter-event time, $\mathbb{E}_\pi [\Delta_i]$. Thus, optimizing the long-run reward rate could be regarded as a fractional optimization problem.

This ratio representation suggests a simple way to reuse the state-level Bellman characterization from Section 2. Let

$$\theta^* := \max_{\pi} \theta(\pi) = \max_{\pi} \frac{\mathbb{E}_\pi [R_i]}{\mathbb{E}_\pi [\Delta_i]} \quad (27)$$

denote the optimal reward rate. Consider the following transformed outcome $\tilde{Y}_i = R_i - \theta^* \Delta_i$. For any policy π ,

$$\mathbb{E}_\pi [\tilde{Y}_i] = \mathbb{E}_\pi [R_i] - \theta^* \mathbb{E}_\pi [\Delta_i] = \mathbb{E}_\pi [\Delta_i] (\theta(\pi) - \theta^*) \leq 0, \quad (28)$$

where the inequality follows from $\mathbb{E}_\pi [\Delta_i] > 0$ and $\theta(\pi) \leq \theta^*$, and equality holds if and only if $\theta(\pi) = \theta^*$. Therefore, the optimal transformed average outcome is zero, and the policies maximizing this transformed average outcome are exactly the reward-rate optimal policies.

We can thus directly apply the state-level Bellman characterization from Section 2.2 to the transformed outcome \tilde{Y}_i . In particular, this amounts to replacing the baseline reward and direct effect in (10) by $r_{\tilde{Y},0}(s) = r_{R,0}(s) - \theta^* r_{\Delta,0}(s)$ and $\tau_{\tilde{Y}}(x, s) = \tau_R(x, s) - \theta^* \tau_\Delta(x, s)$, where $r_{R,0}(s)$, $r_{\Delta,0}(s)$, $\tau_R(x, s)$, $\tau_\Delta(x, s)$ are the state-level average baseline outcomes and CADEs associated with the two outcome variables R_i and Δ_i . The Bellman operator now becomes

$$(T_{S,\theta^*}v)(s) := r_{\tilde{Y},0}(s) + (P_{S,0}v)(s) + \mathbb{E}_X \left[(\tau_{\tilde{Y}}(X, s) + ((P_{S,1} - P_{S,0})v)(s))_+ \right], \quad (29)$$

and an optimal reward-rate policy then takes the form

$$\pi^*(x, s) = I \left(\tau_{\tilde{Y}}(x, s) > - \sum_{s' \in \mathcal{S}} \{P_{S,1}(s' | s) - P_{S,0}(s' | s)\} V^*(s') \right). \quad (30)$$

In practice, since the Bellman operator T_{S,θ^*} depends on the unknown parameter θ^* , we solve the transformed problem by iterating over candidate reward rates. Given a current value $\theta^{(b)}$, we apply Algorithm 1 with the Bellman operator $T_{S,\theta^{(b)}}$ obtained by replacing θ^* in (29) with $\theta^{(b)}$. This yields a greedy policy $\pi^{(b)}$. We then update

$$\theta^{(b+1)} = \frac{\sum_s d_{\pi^{(b)}}(s) (r_{R,0}(s) + \mathbb{E}_X [\pi^{(b)}(X, s) \tau_R(X, s)])}{\sum_s d_{\pi^{(b)}}(s) (r_{\Delta,0}(s) + \mathbb{E}_X [\pi^{(b)}(X, s) \tau_\Delta(X, s)])} \quad (31)$$

and repeat this procedure until the transformed average outcome under $\pi^{(b)}$ is close to zero. This can be viewed as the standard Dinkelbach update for fractional programming [Dinkelbach, 1967], with the inner optimization solved by the Bellman equation for the transformed outcome.

4 Numerical Examples

In this section, we study two queuing simulations motivated by concrete service systems. The first simulation is motivated by emergency-department fast-track triage, where the hospital decides whether to route clinically eligible patients to a fast-track queue or to the regular treatment queue. The second simulation is motivated by online customer support, where the platform decides whether to admit a user to the human-agent queue or route the user to an AI support channel. In the latter setting, users observe the expected wait time for human support before entering the system, so arrivals depend on the current congestion level.

In both settings, we first compare an oracle system-aware targeting rule with a direct CADE targeting rule. These comparisons illustrate the importance of accounting for downstream congestion effects. We then evaluate whether these system-aware rules can be learned from offline data using Algorithm 1. For the state-dependent-arrival customer-support experiment, we use the Dinkelbach-based reward-rate variant introduced in Section 3. We refer to our implementation of Algorithm 1 as state-aware CADE thresholding (SACT) in the figures, and evaluate learned policies in terms of their long-run performance.

We compare SACT with three benchmark methods. The first is a direct targeting rule that estimates the relevant state-aware CADE using a causal forest and assigns treatment whenever the estimated CADE is positive. The remaining two benchmarks are standard batch offline reinforcement-learning algorithms: discrete conservative Q-learning (CQL) [Kumar et al., 2020] and fitted Q-iteration (FQI) [Ernst et al., 2005]. These reinforcement-learning baselines instantiate the collapsed-state paradigm discussed in Section 2.4: they treat the unit attributes and system state as a single Markov state, $Z_i = (X_i, S_i)$, and learn over the resulting covariate-state-action space. Thus, unlike SACT, they do not exploit the exogenous-covariate structure that separates estimation of the state-aware CADE from the lower-dimensional state-level dynamic program. Additional implementation details are provided in Appendix C.

4.1 Emergency Department Fast-Track Routing

Our first numerical example is motivated by fast-track systems in emergency departments. Patients arrive sequentially with observed clinical features, and triage staff must decide whether an eligible patient should be routed to a fast-track treatment stream or to the regular treatment queue. The fast-track stream provides faster service but has limited capacity. Thus, the decision is not simply whether fast-track care benefits the current patient in isolation: routing too many patients to the fast-track stream can congest that queue and reduce its value for future delay-sensitive patients. This is precisely the type of setting where a direct targeting rule may overuse a scarce resource.

We model this setting as a parallel-queue system. Patients arrive according to an exogenous Poisson process and are routed to one of two queues: the regular queue, denoted by $j = 0$, and the fast-track queue, denoted by $j = 1$. Each queue $j \in \{0, 1\}$ has service rate μ_j and maximum capacity \bar{k}_j . The two queues operate independently, with service proceeding whenever the corresponding queue is nonempty. Upon each arrival, we observe the patient’s covariates X_i and the current queue lengths $S_i = (K_{0i}, K_{1i})$. The treatment $W_i = 1$ routes the patient to the fast-track queue, while $W_i = 0$ routes the patient to the regular queue. Additional details on the transition dynamics of this parallel-queue system can be found in Section A.2.

For each patient i , we observe covariates generated as $X_i \sim N(0, I_{10})$. The regular queue has capacity $\bar{k}_0 = 10$, and the fast-track queue has capacity $\bar{k}_1 = 3$. We set the arrival rate to $\lambda = 1$, and the service rates to $\mu_0 = 0.5$ for the regular queue and $\mu_1 = 1$ for the fast-track queue. Thus, the fast-track queue serves patients more quickly, but also has a smaller capacity. Upon patient i ’s arrival, a preliminary treatment $W_i \in \{0, 1\}$ is drawn from a Bernoulli(0.5) behavior policy. At boundary states, this random draw is overridden by the feasibility rule from Section A.2: if one queue is full and the other is not, the patient is routed to the non-full queue; if both modeled queues are full, there is no feasible routing decision at that instant and the arrival is not included as an admitted decision epoch. The outcome Y_i is generated as

$$Y_i = -\log(\text{waiting}_i + \text{service}_i) \cdot \mathbb{I}(X_{i,1} \leq Z_{0.75}) - 3(\text{waiting}_i + \text{service}_i)^2 \cdot \mathbb{I}(X_{i,1} > Z_{0.75}) + \epsilon_i,$$

where $\epsilon_i \sim N(0, 1)$ and $Z_{0.75}$ denotes the 75th percentile of the marginal distribution of $X_{i,1}$. All patients prefer shorter waits, but the top quartile in $X_{i,1}$ is especially delay-sensitive and experiences a quadratic loss from long waiting and service times. Under this setting, the CADE of fast-track routing is positive except when the regular queue is empty and the

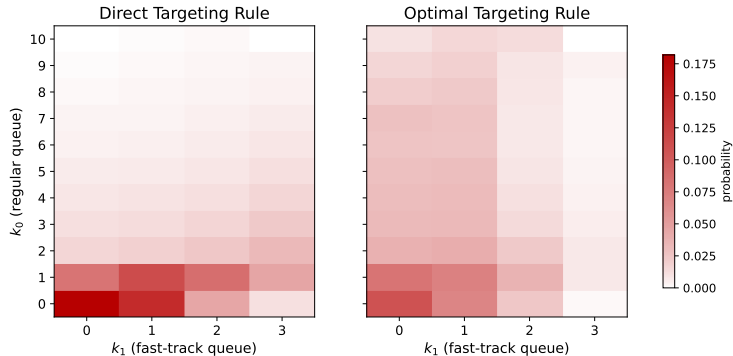


Figure 2: Stationary distribution of queue lengths (K_{0i}, K_{1i}) under the direct targeting rule and the optimal targeting rule. The intensity of the colors represents how often patients experience each combination of queue lengths, with darker colors indicating more frequent occurrences.

fast-track queue is already moderately congested ($K_{0i} = 0$ and $K_{1i} \geq 2$). The CADE can become very large for delay-sensitive patients, particularly when the regular queue is long.

We compare the direct targeting rule with the oracle system-aware targeting rule. Figure 2 shows that the oracle targeting rule changes the queuing system itself. Relative to direct targeting, the oracle rule shifts stationary density away from congested fast-track states such as $(k_0, 3)$ and toward less crowded states with $k_1 \in \{0, 1, 2\}$. This preserves fast-track capacity so that, when delay-sensitive patients arrive, they can be routed promptly. In contrast, the direct targeting rule treats the fast-track queue as beneficial whenever the current patient’s CADE is positive. Because the fast-track CADE is positive for most patient-state pairs, direct targeting tends to overutilize the fast-track queue, resulting in heavier congestion and a more imbalanced state distribution. The performance gap between direct targeting and the oracle benchmark is reported on the same long-run outcome scale in Figure 3.

We now evaluate SACT in this emergency-department routing simulation. Figure 3 summarizes the long-run average outcomes achieved by the learned policies across $n \in \{2000, \dots, 10000\}$ accepted arrivals. The direct targeting rule performs consistently poorly across all sample sizes and exhibits almost no variability across replications. This is because the estimated CADE of fast-track service is nearly always positive, leading the direct method to recover an almost always-treat policy that routes patients to the fast-track queue whenever capacity is available.

Among the benchmark reinforcement-learning methods, FQI performs better than discrete CQL and improves steadily as the sample size increases. Nevertheless, both methods remain substantially below SACT. This pattern is consistent with the fact that the reinforcement-learning baselines must learn values over the full covariate-state-action space, whereas SACT uses the structural result from Theorem 2 to reduce the dynamic component of the problem to state-specific thresholds. The performance of SACT improves steadily as n increases and moves closer to the optimal policy benchmark.

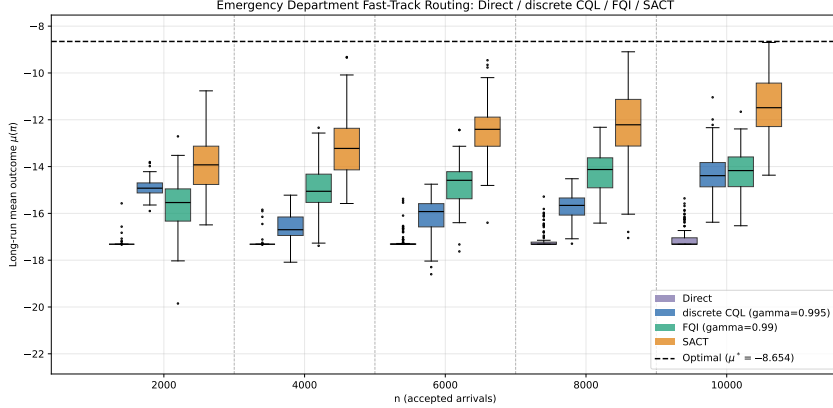


Figure 3: Long-run average outcomes achieved by policies generated using Algorithm 1 and the benchmark methods. The dashed horizontal line represents the optimal long-run average outcome approximated using the ground-truth model together with the policy shown in Figure 2.

4.2 Online Customer Support with Congestion-Sensitive Arrivals

Our second numerical example is motivated by an online platform that provides customer support through two channels: a limited-capacity human-agent queue and an automated AI support channel. A user who needs help first observes an estimated wait time for a human agent and then submits a description of their problem. The platform observes request-level features, such as issue category, urgency, and predicted suitability for automated resolution. The decision is whether to admit the user to the human-agent queue ($W_i = 1$) or route the user to the AI support channel ($W_i = 0$), which is not capacity constrained. The reward is a customer-experience outcome observed for both channels, such as post-interaction satisfaction. This application differs from the emergency-department example because arrivals are congestion-sensitive. When the posted human-agent wait is long, some users defer their request or search help articles instead. The platform’s routing decisions therefore affect not only the satisfaction of users who enter the system, but also the rate at which future users enter.

We model this application using the $M_n/M/1$ queue from Section 3. For each arriving user i , we generate covariates from a 10-dimensional normal distribution, $X_i \sim N(0, I_{10})$, where I_{10} is the 10×10 identity matrix. Let K_i denote the number of users waiting for human support when user i arrives. Routing a user to the AI support channel does not increase this queue. The users’ arrival rate when the queue length is k is $\lambda_k = I(k < 20) \cdot 2/(k + 1)^{0.1}$, and the service rate is $\mu_k = I(k > 0)$, where $k \in \{0, \dots, 20\}$. The decreasing arrival rate captures the idea that users are less likely to enter the human-support flow when the visible backlog is larger. We consider a status-quo policy π_0 that admits user i to the human-agent queue with probability $\pi_0(X_i, K_i)$, where

$$\pi_0(x, k) = 0.6 + 0.2I(x_2 > 0) - 0.1I(x_4 + x_5 > 0), \quad (32)$$

which is unknown to the policy maker. For arriving users, the reward R_i is generated as

$$R_i = W_i \cdot \{(7 - K_i) |X_{i,1}| + 3X_{i,2}\} + 2 \max\{X_{i,3}, 0\} + \epsilon_i, \quad \epsilon_i \sim N(0, 4). \quad (33)$$

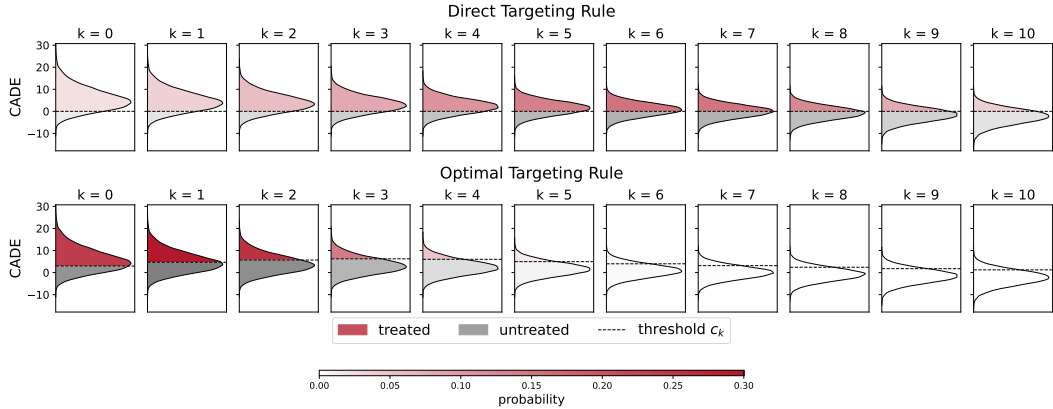


Figure 4: Targeting rules for users arriving at the support system with different human-agent queue lengths ($k = 0, \dots, 10$). The full state space is $k = 0, \dots, 20$; states $k > 10$ are omitted from the display for readability, while optimization and evaluation use all states. The curves in each panel show the distribution of the reward CADE $\tau(X_i, k)$ for users arriving when the queue length is k . The horizontal line represents the effective state-specific threshold for admission to the human-agent queue, which is fixed at zero under the direct targeting rule. The red area shows users admitted to human support, while the grey area shows users routed to the AI support channel. The intensity of the colors represents how often users experience each queue length, with darker colors indicating more frequent occurrences.

The final term $2 \max\{X_{i,3}, 0\}$ is the baseline customer-experience reward under the AI channel. We interpret $X_{i,3}$ as measuring whether the user’s issue is well suited to automated resolution. The term multiplied by W_i is the incremental effect of admitting the user to the human-agent queue. The component $(7 - K_i) |X_{i,1}|$ makes some users especially sensitive to the human-agent wait: when the queue is short, human support can be very valuable for these users, but when $K_i > 7$, the expected delay can make human support worse than immediate AI assistance. The component $3X_{i,2}$ captures issue types for which human discretion is systematically more or less valuable.

A comparison between the oracle policy and the direct targeting policy is illustrated in Figure 4. The oracle policy is more selective in admitting users to the human-agent queue, especially at smaller queue lengths where many users have positive direct effects. This may initially seem counterintuitive, since one might expect a short queue to accommodate more users. However, the objective is a long-run reward rate, and admitting marginally beneficial users can increase future waiting times and reduce the arrival rate faced by the platform. By routing users with lower CADE values to AI support, the oracle policy keeps the human queue short more often and preserves capacity for users with larger gains from timely human assistance.

Next, we examine the policy generated by SACT using the Dinkelbach-based variant introduced in Section 3. We train each method on data observed over a time period of length T and compare its long-run reward rate with the optimal policy benchmark. We compare against the same three baselines as above. To evaluate the long-run reward rate under the learned policies, we compute the conditional CADE distribution with Monte Carlo approximations and the stationary distribution analytically using the formulas provided in

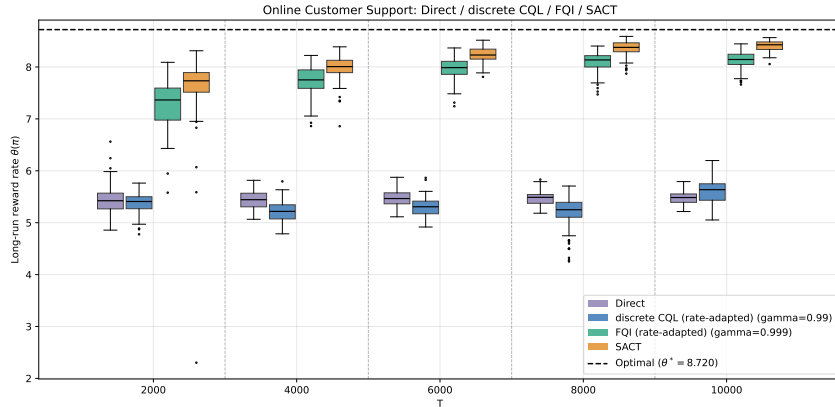


Figure 5: Long-run reward rates achieved by policies generated using Algorithm 1 and the benchmark methods. The dashed horizontal line represents the optimal long-run reward rate obtained using the ground-truth model together with the policy shown in Figure 4.

Section B of the supplementary material. We vary T from 2,000 to 10,000 and repeat the process 100 times for each horizon length considered.

Figure 5 reports the long-run reward rates achieved by the learned policies. As the observation horizon T increases, the performance of SACT steadily improves, with the resulting reward rates approaching the optimal policy benchmark indicated by the dashed line. In contrast, both the direct targeting rule and discrete CQL perform substantially worse across all horizon lengths considered. FQI performs considerably better and benefits from longer trajectories, indicating that it is able to extract useful information from the offline data. Nevertheless, its performance remains consistently below that of SACT. As in the emergency-department example, this comparison uses oracle-tuned discount factors for the reinforcement-learning baselines, whereas SACT directly targets the average-outcome objective in the exogenous-arrival setting and the reward-rate objective in the congestion-sensitive-arrival setting through state-specific thresholds.

5 Discussion

The existing literature on data-driven decision making is largely split into two separate strands. One strand is focused on static, single-action settings where optimal decision can be achieved via reasonably simple thresholding strategies [Athey and Imbens, 2016, Manski, 2004] and/or empirical maximization algorithms [Bertsimas and Kallus, 2020, Kitagawa and Tetenov, 2018]. The other strand considers dynamic decision making problems, for which much more complicated reinforcement learning algorithms are typically used [Lucek et al., 2020, Robins, 2004, Sutton et al., 1999]. And this dichotomy of the literature creates a challenge for practitioners. Ideally, one might imagine building up learning algorithms step by step, where first one learns how to target under a simplified static model and then later accommodates dynamics. But if static vs. dynamic decision-making problems involve completely different algorithmic solutions, then it is not clear whether it’s even possible to “build up” from a static targeting strategy to a dynamic one.

In this paper, we presented some results that help bridge this gap. We found that, in a

class of Markov decision processes, optimal dynamic targeting rules reduce to simple thresholding rules just like in the static case. But, unlike in the static case, decision thresholds are now state dependent and reflect problem dynamics—and deriving optimal thresholds requires leveraging techniques for dynamic off-policy evaluation. Our approach thus paints a clear picture of what it takes to move from static to dynamic targeting solutions; what insights can be kept; and what parts of the algorithm need to be changed to accommodate dynamics. Going forward, we expect it to be of interest to explore other decision-making problems whose difficulty lies “between” basic static problems and fully general dynamic ones; and to investigate practical targeting algorithms that can be deployed in such settings.

References

- Karun Adusumilli, Friedrich Geiecke, and Claudio Schilter. Dynamically optimal treatment allocation. *arXiv preprint arXiv:1904.01047*, 2019.
- Alekh Agarwal, Kianté Brantley, Nan Jiang, Sham M. Kakade, and Wen Sun. Reinforcement learning: Theory and algorithms, 2026. URL <https://rltheorybook.github.io/>. Working draft, version April 11, 2026.
- Shipra Agrawal and Randy Jia. Learning in structured mdps with convex cost functions: Improved regret bounds for inventory management. In *Proceedings of the 2019 ACM Conference on Economics and Computation*, pages 743–744, 2019.
- Abhishek Ananth. Optimal treatment assignment rules on networked populations. Technical report, Working paper, 2020.
- Peter M Aronow and Cyrus Samii. Estimating average causal effects under general interference, with application to a social network experiment. *The Annals of Applied Statistics*, 11(4):1912–1947, 2017.
- Susan Athey and Guido Imbens. Recursive partitioning for heterogeneous causal effects. *Proceedings of the National Academy of Sciences*, 113(27):7353–7360, 2016.
- Susan Athey and Stefan Wager. Policy learning with observational data. *Econometrica*, 89(1):133–161, 2021.
- Susan Athey, Julie Tibshirani, and Stefan Wager. Generalized random forests. *The Annals of Statistics*, 47(2):1148–1178, 2019.
- Gah-Yi Ban and Cynthia Rudin. The big data newsvendor: Practical insights from machine learning. *Operations Research*, 67(1):90–108, 2019.
- Kirk Bansak, Soonbong Lee, Vahideh Manshadi, Rad Niazadeh, and Elisabeth Paulson. Dynamic matching with post-allocation service and its application to refugee resettlement. *arXiv preprint arXiv:2410.22992*, 2024.
- Guillaume W Basse, Avi Feller, and Panos Toulis. Randomization tests of causal effects under interference. *Biometrika*, 106(2):487–494, 2019.
- Dimitris Bertsimas and Nathan Kallus. From predictive to prescriptive analytics. *Management Science*, 66(3):1025–1044, 2020.

- Debopam Bhattacharya and Pascaline Dupas. Inferring welfare maximizing treatment assignment under budget constraints. *Journal of Econometrics*, 167(1):168–196, 2012.
- Christian Borgs, Jennifer T Chayes, Sherwin Doroudi, Mor Harchol-Balter, and Kuang Xu. The optimal admission threshold in observable queues with state dependent pricing. *Probability in the Engineering and Informational Sciences*, 28(1):101–119, 2014.
- Justin Boutilier, Jonas Oddur Jonasson, Hannah Li, and Erez Yoeli. Randomized controlled trials of service interventions: The impact of capacity constraints. *arXiv preprint arXiv:2407.21322*, 2024.
- Defu Cao and Angela Zhou. Orthogonalized estimation of difference of q -functions. *arXiv preprint arXiv:2406.08697*, 2024.
- Boxiao Chen, Jiashuo Jiang, Jiawei Zhang, and Zhengyuan Zhou. Learning to order for inventory systems with lost sales and uncertain supplies. *Management Science*, 70(12):8631–8646, 2024.
- Hong Chen and Murray Z Frank. State dependent pricing with a queue. *IIE Transactions*, 33(10):847–860, 2001.
- Xi Chen, Zachary Owen, Clark Pixton, and David Simchi-Levi. A statistical learning approach to personalization in revenue management. *Management Science*, 68(3):1923–1937, 2022.
- Victor Chernozhukov, Denis Chetverikov, Mert Demirer, Esther Duflo, Christian Hansen, Whitney Newey, and James Robins. Double/debiased machine learning for treatment and structural parameters, 2018.
- Victor Chernozhukov, Juan Carlos Escanciano, Hidehiko Ichimura, Whitney K Newey, and James M Robins. Locally robust semiparametric estimation. *Econometrica*, 90(4):1501–1535, 2022.
- Wang Chi Cheung and David Simchi-Levi. Sampling-based approximation schemes for capacitated stochastic inventory control models. *Mathematics of Operations Research*, 44(2):668–692, 2019.
- Thomas Dietterich, George Trimonias, and Zhitang Chen. Discovering and removing exogenous state variables and rewards for reinforcement learning. In *International Conference on Machine Learning*, pages 1262–1270. PMLR, 2018.
- Jingying Ding, Woonghee Tim Huh, and Ying Rong. Feature-based inventory control with censored demand. *Manufacturing & Service Operations Management*, 26(3):1157–1172, 2024.
- Werner Dinkelbach. On nonlinear fractional programming. *Management Science*, 13(7):492–498, 1967.
- Yonathan Efroni, Dylan J Foster, Dipendra Misra, Akshay Krishnamurthy, and John Langford. Sample-efficient reinforcement learning in the presence of exogenous information. In *Conference on Learning Theory*, pages 5062–5127. PMLR, 2022.

- Damien Ernst, Pierre Geurts, and Louis Wehenkel. Tree-based batch mode reinforcement learning. *Journal of Machine Learning Research*, 6, 2005.
- Eyal Even-Dar, Sham M Kakade, and Yishay Mansour. Online markov decision processes. *Mathematics of Operations Research*, 34(3):726–736, 2009.
- Vivek Farias, Andrew Li, Tianyi Peng, and Andrew Zheng. Markovian interference in experiments. *Advances in Neural Information Processing Systems*, 35:535–549, 2022.
- Max H Farrell, Tengyuan Liang, and Sanjog Misra. Deep neural networks for estimation and inference. *Econometrica*, 89(1):181–213, 2021.
- Qi Feng and J George Shanthikumar. How research in production and operations management may evolve in the era of big data. *Production and Operations Management*, 27(9):1670–1684, 2018.
- Andrea Galeotti, Benjamin Golub, and Sanjeev Goyal. Targeting interventions in networks. *Econometrica*, 88(6):2445–2471, 2020.
- Miguel A Hernán and James M Robins. *Causal Inference: What If*. Chapman & Hall/CRC, Boca Raton, 2020.
- Keisuke Hirano and Jack R Porter. Asymptotics for statistical treatment rules. *Econometrica*, 77(5):1683–1701, 2009.
- Ronald A Howard. *Dynamic Programming and Markov Processes*. John Wiley and Sons/MIT Press, 1960.
- Yuchen Hu, Shuangning Li, and Stefan Wager. Average direct and indirect causal effects under interference. *Biometrika*, 109(4):1165–1172, 2022.
- Xinyang Huang and Jin Xu. Estimating individualized treatment rules with risk constraint. *Biometrics*, 76(4):1310–1318, 2020.
- Michael G Hudgens and M Elizabeth Halloran. Toward causal inference with interference. *Journal of the American Statistical Association*, 103(482):832–842, 2008.
- Peter S Hussey, Jeanne S Ringel, Sangeeta Ahluwalia, Rebecca Anhang Price, Christine Buttorff, Thomas W Concannon, Susan L Lovejoy, Grant R Martsoff, Robert S Rudin, Dana Schultz, et al. Resources and capabilities of the department of veterans affairs to provide timely and accessible care to veterans. *Rand Health Quarterly*, 5(4), 2016.
- Kosuke Imai and Michael Lingzhi Li. Experimental evaluation of individualized treatment rules. *Journal of the American Statistical Association*, 118(541):242–256, 2023.
- Evin Uzun Jacobson, Nilay Tanık Argon, and Serhan Ziya. Priority assignment in emergency response. *Operations Research*, 60(4):813–832, 2012.
- Ying Jin, Ramki Gummadi, Zhengyuan Zhou, and Jose Blanchet. Feasible q -learning for average reward reinforcement learning. In *International Conference on Artificial Intelligence and Statistics*, pages 1630–1638. PMLR, 2024.
- Søren Glud Johansen and Shaler Stidham Jr. Control of arrivals to a stochastic input–output system. *Advances in Applied Probability*, 12(4):972–999, 1980.

- Ramesh Johari, Hannah Li, Anushka Murthy, and Gabriel Y Weintraub. When does interference matter? decision-making in platform experiments. *arXiv preprint arXiv:2410.06580*, 2024.
- Ramesh Johari, Tianyi Peng, and Wenqian Xing. Estimation of treatment effects under nonstationarity via truncated difference-in-q’s. *arXiv preprint arXiv:2506.05308*, 2025.
- Nathan Kallus. Balanced policy evaluation and learning. *Advances in neural information processing systems*, 31, 2018.
- Nathan Kallus and Angela Zhou. Minimax-optimal policy learning under unobserved confounding. *Management Science*, 67(5):2870–2890, 2021.
- Nathan Kallus and Angela Zhou. Stateful offline contextual policy evaluation and learning. In *Proceedings of The 25th International Conference on Artificial Intelligence and Statistics*, volume 151 of *Proceedings of Machine Learning Research*, pages 11169–11194. PMLR, 2022.
- Michael Kearns and Satinder Singh. Near-optimal reinforcement learning in polynomial time. *Machine learning*, 49(2):209–232, 2002.
- Edward H Kennedy. Towards optimal doubly robust estimation of heterogeneous causal effects. *Electronic Journal of Statistics*, 17(2):3008–3049, 2023.
- Edward H Kennedy, Sivaraman Balakrishnan, James M Robins, and Larry Wasserman. Minimax rates for heterogeneous causal effect estimation. *Annals of statistics*, 52(2):793, 2024.
- N Bora Keskin and Can Zhang. Feature-based scheduling and dynamic learning with a large backlog. *Available at SSRN 4852356*, 2024.
- Toru Kitagawa and Aleksey Tetenov. Who should be treated? empirical welfare maximization methods for treatment choice. *Econometrica*, 86(2):591–616, 2018.
- Toru Kitagawa and Guanyi Wang. Individualized treatment allocation in sequential network games. *arXiv preprint arXiv:2302.05747*, 2023a.
- Toru Kitagawa and Guanyi Wang. Who should get vaccinated? individualized allocation of vaccines over sir network. *Journal of Econometrics*, 232(1):109–131, 2023b.
- Aviral Kumar, Aurick Zhou, George Tucker, and Sergey Levine. Conservative q-learning for offline reinforcement learning. *Advances in neural information processing systems*, 33: 1179–1191, 2020.
- Sören R Künzel, Jasjeet S Sekhon, Peter J Bickel, and Bin Yu. Metalearners for estimating heterogeneous treatment effects using machine learning. *Proceedings of the national academy of sciences*, 116(10):4156–4165, 2019.
- Hoang Le, Cameron Voloshin, and Yisong Yue. Batch policy learning under constraints. In *International Conference on Machine Learning*, pages 3703–3712. PMLR, 2019.
- Michael P Leung. Rate-optimal cluster-randomized designs for spatial interference. *The Annals of Statistics*, 50(5):3064–3087, 2022.

- Shuangning Li and Stefan Wager. Random graph asymptotics for treatment effect estimation under network interference. *The Annals of Statistics*, 50(4):2334–2358, 2022.
- Shuangning Li, Ramesh Johari, Xu Kuang, and Stefan Wager. Experimenting under stochastic congestion. *arXiv preprint arXiv:2302.12093*, 2023.
- Daniel J Lockett, Eric B Laber, Anna R Kahkoska, David M Maahs, Elizabeth Mayer-Davis, and Michael R Kosorok. Estimating dynamic treatment regimes in mobile health using V-learning. *Journal of the american statistical association*, 2020.
- Alex Luedtke and Antoine Chambaz. Performance guarantees for policy learning. *Annales de l’IHP Probabilites et statistiques*, 56(3):2162, 2020.
- Alexander R Luedtke and Mark J van der Laan. Optimal individualized treatments in resource-limited settings. *The International Journal of Biostatistics*, 12(1):283–303, 2016.
- Charles F. Manski. Statistical treatment rules for heterogeneous populations. *Econometrica*, 72(4):1221–1246, 2004. doi: <https://doi.org/10.1111/j.1468-0262.2004.00530.x>.
- Charles F Manski. *Identification for prediction and decision*. Harvard University Press, 2009.
- Charles F Manski. Identification of treatment response with social interactions. *The Econometrics Journal*, 16(1):S1–S23, 2013.
- P. Marbach and J.N. Tsitsiklis. Simulation-based optimization of markov reward processes. *IEEE Transactions on Automatic Control*, 46(2):191–209, 2001.
- Harvey W Meislin, Sally A Coates, Janine Cyr, and Terry Valenzuela. Fast track: Urgent care within a teaching hospital emergency department: Can it work? *Annals of Emergency Medicine*, 17(5):453–456, 1988.
- Alex F Mills, Nilay Tanik Argon, and Serhan Ziya. Resource-based patient prioritization in mass-casualty incidents. *Manufacturing & Service Operations Management*, 15(3):361–377, 2013.
- Evan Munro, Xu Kuang, and Stefan Wager. Treatment effects in market equilibrium. *American Economic Review*, 115(10):3273–3321, 2025.
- Susan A Murphy. Optimal dynamic treatment regimes. *Journal of the Royal Statistical Society: Series B (Statistical Methodology)*, 65(2):331–355, 2003.
- Susan A Murphy. A generalization error for q-learning. *Journal of Machine Learning Research*, 6:1073–1097, 2005.
- Karthyeek Murthy, Divya Padmanabhan, and Satyanath Bhat. Admission control in the presence of arrival forecasts with blocking-based policy optimization. In *2022 Winter Simulation Conference (WSC)*, pages 2270–2281. IEEE, 2022.
- Pinhas Naor. The regulation of queue size by levying tolls. *Econometrica*, 37(1):15–24, 1969.
- Xinkun Nie and Stefan Wager. Quasi-oracle estimation of heterogeneous treatment effects. *Biometrika*, 108(2):299–319, 2021.

- Xinkun Nie, Emma Brunskill, and Stefan Wager. Learning when-to-treat policies. *Journal of the American Statistical Association*, 116(533):392–409, 2021.
- Michael JD Powell. *A Direct Search Optimization Method That Models the Objective and Constraint Functions by Linear Interpolation*, pages 51–67. Springer Netherlands, Dordrecht, 1994.
- Michael JD Powell. Direct search algorithms for optimization calculations. *Acta numerica*, 7:287–336, 1998.
- Martin L. Puterman. *Markov Decision Processes: Discrete Stochastic Dynamic Programming*. Wiley, 1994.
- Min Qian and Susan A Murphy. Performance guarantees for individualized treatment rules. *Annals of Statistics*, 39(2):1180, 2011.
- James M Robins. Optimal structural nested models for optimal sequential decisions. In *Proceedings of the second seattle Symposium in Biostatistics*, pages 189–326. Springer, 2004.
- Sheldon Ross. *Introduction to Probability Models (Eleventh Edition)*. Academic Press, Boston, eleventh edition edition, 2014.
- Fredrik Sävje, Peter M Aronow, and Michael G Hudgens. Average treatment effects in the presence of unknown interference. *The Annals of Statistics*, 49(2):673–701, 2021.
- Yunting Shi, Nan Liu, and Guohua Wan. Treatment planning for victims with heterogeneous time sensitivities in mass casualty incidents. *Operations Research*, 72(4):1400–1420, 2024.
- Sean R Sinclair, Felipe Vieira Frujeri, Ching-An Cheng, Luke Marshall, Hugo De Oliveira Barbalho, Jingling Li, Jennifer Neville, Ishai Menache, and Adith Swaminathan. Hind-sight learning for mdps with exogenous inputs. In *International Conference on Machine Learning*, pages 31877–31914. PMLR, 2023.
- Jörg Stoye. Minimax regret treatment choice with finite samples. *Journal of Econometrics*, 151(1):70–81, 2009.
- Jörg Stoye. Minimax regret treatment choice with covariates or with limited validity of experiments. *Journal of Econometrics*, 166(1):138–156, 2012.
- Hao Sun, Evan Munro, Georgy Kalashnov, Shuyang Du, and Stefan Wager. Treatment allocation under uncertain costs. *arXiv preprint arXiv:2103.11066*, 2021.
- Liyang Sun. Empirical welfare maximization with constraints. *arXiv preprint arXiv:2103.15298*, 2, 2021.
- Richard S. Sutton and Andrew G. Barto. *Reinforcement Learning: An Introduction*. A Bradford Book, Cambridge, MA, USA, 2018. ISBN 0262039249.
- Richard S Sutton, David McAllester, Satinder Singh, and Yishay Mansour. Policy gradient methods for reinforcement learning with function approximation. *Advances in neural information processing systems*, 12, 1999.

- Erik Sverdrup, Han Wu, Susan Athey, and Stefan Wager. Qini curves for multi-armed treatment rules. *Journal of Computational and Graphical Statistics*, pages 1–13, 2024.
- Eric J Tchetgen Tchetgen and Tyler J VanderWeele. On causal inference in the presence of interference. *Statistical Methods in Medical Research*, 21(1):55–75, 2012.
- Aleksey Tetenov. Statistical treatment choice based on asymmetric minimax regret criteria. *Journal of Econometrics*, 166(1):157–165, 2012. doi: <https://doi.org/10.1016/j.jeconom.2011.06.013>.
- Benjamin Van Roy. *Learning and Value Function Approximation in Complex Decision Processes*. PhD thesis, Massachusetts Institute of Technology, 1998.
- Pauli Virtanen, Ralf Gommers, Travis E Oliphant, Matt Haberland, Tyler Reddy, David Cournapeau, Evgeni Burovski, Pearu Peterson, Warren Weckesser, Jonathan Bright, et al. Scipy 1.0: fundamental algorithms for scientific computing in python. *Nature methods*, 17(3):261–272, 2020.
- Davide Viviano. Policy targeting under network interference. *Review of Economic Studies*, page rdae041, 2024.
- Stefan Wager. Causal inference: A statistical learning approach, 2025.
- Jia Wan, Sean R Sinclair, Devavrat Shah, and Martin J Wainwright. Exploiting exogenous structure for sample-efficient reinforcement learning. *arXiv preprint arXiv:2409.14557*, 2024.
- Yuanjia Wang, Haoda Fu, and Donglin Zeng. Learning optimal personalized treatment rules in consideration of benefit and risk: with an application to treating type 2 diabetes patients with insulin therapies. *Journal of the American Statistical Association*, 113(521): 1–13, 2018.
- Honghao Wei, Xin Liu, Weina Wang, and Lei Ying. Sample efficient reinforcement learning in mixed systems through augmented samples and its applications to queueing networks. In *Advances in Neural Information Processing Systems*, volume 36, 2023.
- Kuang Xu and Carri W Chan. Using future information to reduce waiting times in the emergency department via diversion. *Manufacturing & Service Operations Management*, 18(3):314–331, 2016.
- Yizhe Xu, Tom H Greene, Adam P Bress, Brian C Sauer, Brandon K Bellows, Yue Zhang, William S Weintraub, Andrew E Moran, and Jincheng Shen. Estimating the optimal individualized treatment rule from a cost-effectiveness perspective. *Biometrics*, 78(1): 337–351, 2022.
- Steve Yadlowsky, Scott Fleming, Nigam Shah, Emma Brunskill, and Stefan Wager. Evaluating treatment prioritization rules via rank-weighted average treatment effects. *Journal of the American Statistical Association*, 120(549):38–51, 2025.
- Nur Hani Zainal, Robert M. Bossarte, Sarah M. Gildea, Irving Hwang, Chris J. Kennedy, Howard Liu, Alex Luedtke, Brian P. Marx, Maria V. Petukhova, Edward P. Post, Eric L. Ross, Nancy A. Sampson, Erik Sverdrup, Brett Turner, Stefan Wager, and Ronald C. Kessler. Developing an individualized treatment rule for veterans with major depressive disorder using electronic health records. *Molecular Psychiatry*, 29(8):2335–2345, 2024.

- Ruohan Zhan, Shichao Han, Yuchen Hu, and Zhenling Jiang. Estimating treatment effects under recommender interference: A structured neural networks approach. *arXiv preprint arXiv:2406.14380*, 2024.
- Baqun Zhang, Anastasios A Tsiatis, Eric B Laber, and Marie Davidian. Robust estimation of optimal dynamic treatment regimes for sequential treatment decisions. *Biometrika*, 100(3):681–694, 2013.
- Yi Zhang and Kosuke Imai. Individualized policy evaluation and learning under clustered network interference. *arXiv preprint arXiv:2311.02467*, 2023.
- Yiming Zhang and Keith W Ross. On-policy deep reinforcement learning for the average-reward criterion. In *International Conference on Machine Learning*, pages 12535–12545. PMLR, 2021.
- Zhengyuan Zhou, Susan Athey, and Stefan Wager. Offline multi-action policy learning: Generalization and optimization. *Operations Research*, 71(1):148–183, 2023.
- Matthew Zurek and Yudong Chen. The plug-in approach for average-reward and discounted mdps: Optimal sample complexity analysis. *arXiv preprint arXiv:2410.07616*, 2024.

Supplemental Materials

A Application: Optimal Targeting in Queuing Systems

In this section, we instantiate the general framework developed in Section 2 in the context of queuing systems. We begin with a simple admission problem in an $M/M/1$ queue with finite capacity \bar{k} ,⁵ where the policy determines which units are admitted into the queue. We then discuss how the same approach extends to parallel queues, where the policy routes each arriving unit to one of several service tracks. These examples illustrate how the state-aware CADE thresholding rule accounts for the downstream congestion effects induced by current admission decisions.

A.1 Targeting in a Simple Queuing Model

Consider an $M/M/1$ queue in which patients arrive at rate λ and are served at rate μ , where both rates are bounded and bounded away from zero [Ross, 2014]. We observe a sequence of n patient arrivals, indexed by $i = 1, \dots, n$, under a status quo behavior policy π_0 , which could be potentially unobserved. When patient i arrives, we observe their covariates $X_i \in \mathcal{X}$ and the current queue length $K_i = 0, 1, \dots, \bar{k}$. The system then assigns treatment $W_i \in \{0, 1\}$, where $W_i = 1$ corresponds to admitting the patient into the queue and $W_i = 0$ corresponds to assigning the patient to the outside option. We record the outcome Y_i , which may depend on the patient’s covariates, the treatment assignment, and the queue length at the time of arrival.⁶ As in Assumption 2, we assume that Y_i is bounded almost surely.

In such a queuing system, the queue length K_i plays the role of the system state. Conditional on the current queue length and treatment assignment, the next queue length is determined by whether the current patient is admitted and by the number of service completions before the next arrival. Thus, when the process is observed at arrival epochs, $\{K_i\}$ forms a finite-state Markov chain whose transition kernel depends on the current queue length and action. In this way, the simple queuing model satisfies the exogenous-covariate Markov structure in Assumption 1, with $S_i = K_i$.

In this setting, Theorem 2 implies that an optimal admission policy takes the form $\pi^*(x, k) = I(\tau(x, k) > c_k)$, where the threshold c_k depends on the current queue length. Admitting the current patient affects not only that patient’s outcome, but also the queue-length process faced by future arrivals until subsequent service completions relieve the system, and the threshold c_k internalizes this downstream congestion effect. Thus, the state-aware rule may reject a patient with positive direct benefit, not because the treatment is individually harmful, but because the capacity used by that admission has greater expected value for future arrivals. Algorithm 1 can then be applied directly with $S_i = K_i$. In particular, we estimate the CADE $\tau(x, k)$, the baseline reward $r_0(k)$, and the queue-length transition kernels $P_{K,w}(\cdot | k)$, and then run relative value iteration over the finite queue-length state space.

⁵Alternatively, the system can be viewed as a queue without capacity constraints under a policy that assigns patients to control whenever the queue length reaches \bar{k} .

⁶Although Y_i may depend on the realized waiting time, under an $M/M/1$ queue with a state-independent service rate μ , the distribution of the realized waiting time for an admitted patient is determined by the queue length at the time of arrival and the admission decision. Thus, the conditional law of Y_i can still be written as a function of (X_i, K_i, W_i) , as required by Assumption 1.

When the maximum queue length \bar{k} is large, modeling the thresholds c_k as functions of k can sometimes lead to improved finite-sample performance. This parallels common practice in policy learning for MDPs, where treatment probabilities $\pi(x, k)$ are often modeled as functions of both x and k [Sutton and Barto, 2018]. As in those settings, parametrization introduces additional approximation error depending on how well the chosen functional form captures the true thresholds. However, since our policy space is much simpler than that of general MDPs, the quality of approximation is often better in practice.

A.2 Optimal Routing with Parallel Queues

In the basic setting considered above, the policy determines whether to admit an individual into a single queue. In many practical systems, however, individuals can be routed to parallel queues with different service speeds, and the decision lies in routing each arriving individual to one of the available service tracks. For example, in emergency departments, triage nurses need to decide whether to route a patient to a fast-track urgent care line or a regular treatment line; similarly, in online delivery platforms, the system needs to decide whether to assign a customer to expedited delivery or assign them to standard delivery.

We show how our framework can be extended to accommodate such parallel queuing systems by augmenting the state space, where routing decisions influence not only individual outcomes but also system dynamics in both of the queues. In such a parallel queuing system, individuals arrive according to a Poisson process with rate λ and are routed to one of two queues, where each queue $j \in \{0, 1\}$ has its own service rate μ_j and maximum capacity \bar{k}_j . The two queues operate independently, and service proceeds only if the respective queue is non-empty.

Upon each admissible arrival, we observe the individual’s covariate X_i as well as the current queue lengths (K_{0i}, K_{1i}) , and assign a treatment $W_i \sim \pi(X_i, K_{0i}, K_{1i})$ indicating whether the individual is routed to queue 0 or 1. When both queues have available capacity, the policy chooses where to route the individual. If one queue is full and the other is not, the individual is routed to the non-full queue; if both queues are full, potential arrivals are blocked by capacity and are not included in the decision process. Thus, the learned threshold rule is applied only at states where both routing actions are feasible, while boundary decisions are determined by the capacity constraints. After assignment, we record the outcome Y_i , which could depend on the individual’s covariates and the realized wait and service times in the assigned queue. As before, we assume Y_i is bounded almost surely.

To verify that our framework applies to this setting, we note that this is a discrete-time Poisson point process observed at admissible arrivals. Under a fixed routing policy $W_i \sim \pi$, the evolution of the queue lengths (K_{0i}, K_{1i}) follows a time-homogeneous Markov decision process such that

$$\begin{aligned} K_{0,i+1} &= K_{0i} + (1 - W_i) \cdot I(K_{0i} < \bar{k}_0) + W_i \cdot I(K_{1i} = \bar{k}_1) - N_{\text{served},0,i}, \\ K_{1,i+1} &= K_{1i} + W_i \cdot I(K_{1i} < \bar{k}_1) + (1 - W_i) \cdot I(K_{0i} = \bar{k}_0) - N_{\text{served},1,i}, \end{aligned} \tag{S1}$$

where $N_{\text{served},0,i}$ and $N_{\text{served},1,i}$ denote the actual numbers of individuals served between the i th and the $i + 1$ th admissible arrivals in queue 0 and queue 1. We refer readers to Section B of the supplementary material for details on the state dynamics of this system.

Since arrivals and services follow Poisson processes, this embedded process recorded at arrivals satisfies Assumptions 1-2. Algorithm 1 can then be applied directly with $S_i = (K_{0i}, K_{1i})$. In Section 4.1, we demonstrate through simulations that the extended algo-

gorithm learns a system-aware targeting policy that always outperforms the direct targeting benchmark and converges toward the optimal policy as the sample size increases.

Remark 2. By augmenting the state space, our framework can also accommodate dynamic resource allocation problems. Upon each arrival, the system observes both the current resource level and the covariates of the incoming individual including their resource demand, and must decide whether to approve the request. This setup fits naturally into our framework by defining the state as the pair of the current resource level and the individual's demand. This formulation also captures scenarios with multiple types of operations that require different service times (e.g., major versus minor medical procedures, long-distance versus short-distance deliveries), where each type corresponds to a different resource demand level of the service.

B Closed Forms of Transition Kernels and Stationary Distributions

In this section, we derive the closed forms of transition kernels and stationary distributions for the queuing processes considered in the paper. We start with the transition kernel and stationary distribution of the embedded point process recorded at both arrivals and services corresponding to the $M_n/M/1$ system discussed in Section 3, with the standard $M/M/1$ model in Appendix A.1 as a special case. We then show that it is possible to find the stationary distribution of the embedded point process recorded only at arrivals using the stationary distribution of the embedded point process recorded at both arrivals and services. Finally, we derive the closed forms of transition kernels of the parallel queuing system discussed in Section A.2, which provides foundation for approximating its stationary distribution computationally.

B.1 Transition Kernel and Stationary Distribution of an $M_n/M/1$ system

For the embedded point process recorded at both arrivals and services, the state S_i contains both the event type A_i and the queue length K_i . Recall that $A_i = 1$ represents arrivals (i.e., a unit arriving at the system) while $A_i = 0$ represents services (i.e., a unit leaving the system). Let $\bar{\pi}(k) = \mathbb{E}[\pi(X_i, K_i) \mid K_i = k, A_i = 1]$ be the probability of assigning a unit to the queue given current queue length k .

First, we note that $P_S^\pi(s' \mid s)$, the system's transition kernel under policy π , can be written as

$$\begin{aligned}
& P_S^\pi(s' \mid s) \\
&= P_S^\pi(a', k' \mid a, k) \\
&= \bar{\pi}(k) \mathbb{P}[A_{i+1} = a', K_{i+1} = k' \mid A_i = a, K_i = k, W_i = 1] \\
&\quad + (1 - \bar{\pi}(k)) \mathbb{P}[A_{i+1} = a', K_{i+1} = k' \mid A_i = a, K_i = k, W_i = 0] \\
&= \bar{\pi}(k) \mathbb{P}[K_{i+1} = k' \mid A_i = a, K_i = k, W_i = 1] \mathbb{P}[A_{i+1} = a' \mid K_{i+1} = k'] \\
&\quad + (1 - \bar{\pi}(k)) \mathbb{P}[K_{i+1} = k' \mid A_i = a, K_i = k, W_i = 0] \mathbb{P}[A_{i+1} = a' \mid K_{i+1} = k'],
\end{aligned} \tag{S2}$$

where the last equality holds because the probability that the next event is an arrival or not

depends only on the current queue length. Furthermore,

$$\mathbb{P}[A_i = a \mid K_i = k] = \begin{cases} \lambda_k I(k < \bar{k}) / (\lambda_k I(k < \bar{k}) + \mu I(k > 0)) & \text{if } a = 1 \\ \mu I(k > 0) / (\lambda_k I(k < \bar{k}) + \mu I(k > 0)) & \text{if } a = 0. \end{cases} \quad (\text{S3})$$

To derive $\mathbb{P}[K_{i+1} = k' \mid A_i = a, K_i = k, W_i = w]$, observe that the queue length at the next event is deterministic given the current queue length, the event type, and the treatment assignment. In particular, the probability above is nonzero (and equal to one) only in the following cases:

- If $a = 0$ and $k' = k - 1$, then the most recent event is a service completion, which decreases the queue length by one.
- If $a = 1$, $w = 0$ and $k' = k$, then the most recent event is an arrival, but the unit is not assigned to the queue. Thus, the queue length remains unchanged.
- If $a = 1$, $w = 1$ and $k' = k + 1$, then the most recent event is an arrival and the unit is assigned to the queue. Thus, the queue length increases by one.

Putting everything together,

$$P_S^\pi(a', k' \mid a, k) = \begin{cases} \bar{\pi}(k) \mathbb{P}[A_i = a' \mid K_i = k + 1] & \text{if } a = 1, k' = k + 1 \\ (1 - \bar{\pi}(k)) \mathbb{P}[A_i = a' \mid K_i = k] & \text{if } a = 1, k' = k \\ \mathbb{P}[A_i = a' \mid K_i = k - 1] & \text{if } a = 0, k' = k - 1 \\ 0, & \text{otherwise,} \end{cases} \quad (\text{S4})$$

where the form of $\mathbb{P}[A_i = a \mid K_i = k]$ is given in (S3).

To compute the stationary distribution $d_\pi(a, k)$, notice that the next event type is sampled independently of the past given the queue length. This allows us to first focus on the dynamics of the queue lengths only and derive $d^\dagger(k)$. $d(a, k)$ could then be computed as

$$d(a, k) = d^\dagger(k) \cdot \mathbb{P}[A_i = a \mid K_i = k]. \quad (\text{S5})$$

Since the number of states is finite, solving the corresponding system of equations to obtain the stationary distribution is straightforward, with

$$d^\dagger(k) = \frac{r_k}{\sum_{m=0}^{\bar{k}} r_m}, \quad k = 0, \dots, \bar{k}, \quad (\text{S6})$$

and

$$\begin{aligned} r_0 &= 1, \\ r_1 &= \frac{(\lambda_1 + \mu) \bar{\pi}_0}{\mu}, \\ r_k &= \frac{(\lambda_k + \mu) \bar{\pi}_0}{\mu} \prod_{m=1}^{k-1} \frac{\lambda_m \bar{\pi}_m}{\mu}, \quad k = 2, \dots, \bar{k} - 1, \\ r_{\bar{k}} &= \bar{\pi}_0 \prod_{m=1}^{\bar{k}-1} \frac{\lambda_m \bar{\pi}_m}{\mu}. \end{aligned} \quad (\text{S7})$$

B.2 Stationary Distribution of Embedded Point Process Recorded at Arrivals

To find the stationary distribution of the embedded point process recorded only at arrivals, we note that this process further conditions on the event being an arrival. Thus, its stationary distribution could be expressed and computed as

$$\begin{aligned}\mathbb{P}_\pi [K = k \mid A = 1] &= \frac{\mathbb{P}_\pi [K = k, A = 1]}{\sum_{k'=0}^{\bar{k}} \mathbb{P}_\pi [K = k', A = 1]} \\ &= \frac{d(1, k)}{\sum_{k'=0}^{\bar{k}} d(1, k')}.\end{aligned}\tag{S8}$$

B.3 Parallel Queue with Routing

Let the state be (A, K_0, K_1) , where $A = 0$ and $A = 1$ represent service at queues 0 and 1, respectively, and $A = 2$ represents an arrival. For simplicity, we further denote

$$f_{A \mid K_0, K_1}(a \mid k_0, k_1) := \mathbb{P}[A_i = a \mid K_{0i} = k_0, K_{1i} = k_1].$$

It is possible to write down the transition kernel for this setting:

$$P_S(a', k'_0, k'_1 \mid 2, k_0, k_1, w) = \begin{cases} f_{A \mid K_0, K_1}(a' \mid k'_0, k'_1) & \text{if } k'_0 = k_0 + 1, k'_1 = k_1, w = 0 \\ f_{A \mid K_0, K_1}(a' \mid k'_0, k'_1) & \text{if } k'_0 = k_0, k'_1 = k_1 + 1, w = 1 \\ 0, & \text{otherwise,} \end{cases}$$

$$P_S(a', k'_0, k'_1 \mid 0, k_0, k_1, w) = \begin{cases} f_{A \mid K_0, K_1}(a' \mid k'_0, k'_1) & \text{if } k'_0 = k_0 - 1, k'_1 = k_1, k_0 > 0 \\ 0, & \text{otherwise,} \end{cases}$$

and

$$P_S(a', k'_0, k'_1 \mid 1, k_0, k_1, w) = \begin{cases} f_{A \mid K_0, K_1}(a' \mid k'_0, k'_1) & \text{if } k'_0 = k_0, k'_1 = k_1 - 1, k_1 > 0 \\ 0, & \text{otherwise,} \end{cases}$$

where

$$f_{A \mid K_0, K_1}(a \mid k_0, k_1) = \begin{cases} \tilde{\lambda}/(\tilde{\lambda} + \mu_0 I(k_0 > 0) + \mu_1 I(k_1 > 0)) & \text{if } a = 2 \\ \mu_0 I(k_0 > 0)/(\tilde{\lambda} + \mu_0 I(k_0 > 0) + \mu_1 I(k_1 > 0)) & \text{if } a = 0 \\ \mu_1 I(k_1 > 0)/(\tilde{\lambda} + \mu_0 I(k_0 > 0) + \mu_1 I(k_1 > 0)) & \text{if } a = 1, \end{cases}$$

and $\tilde{\lambda} = \lambda \cdot I(k_0 < \bar{k}_0 \text{ or } k_1 < \bar{k}_1)$. The system's transition kernel under policy π can be thus expressed as follows:

$$P_S^\pi(a', k'_0, k'_1 \mid a, k_0, k_1) = \begin{cases} \bar{\pi}(k_0, k_1) f_A(a' \mid k_0, k_1 + 1) & \text{if } a = 2, k'_0 = k_0, k'_1 = k_1 + 1 \\ (1 - \bar{\pi}(k_0, k_1)) f_A(a' \mid k_0 + 1, k_1) & \text{if } a = 2, k'_0 = k_0 + 1, k'_1 = k_1 \\ f_A(a' \mid k_0, k_1 - 1) & \text{if } a = 1, k'_0 = k_0, k'_1 = k_1 - 1, k_1 > 0 \\ f_A(a' \mid k_0 - 1, k_1) & \text{if } a = 0, k'_0 = k_0 - 1, k'_1 = k_1, k_0 > 0 \\ 0, & \text{otherwise.} \end{cases}$$

C Simulation Details

This section provides implementation details for the simulation studies in Section 4.

C.1 Oracle Benchmarks

For the oracle comparisons in Figures 2 and 4, the direct targeting rule thresholds the true state-aware CADE at zero. The oracle system-aware rule is obtained by searching over threshold policies and evaluating each candidate under the ground-truth queuing model.

In the emergency-department experiment, we search over state-specific threshold policies using the COBYLA algorithm [Powell, 1994, 1998], as implemented in `scipy.optimize.minimize` from the Python SciPy package [Virtanen et al., 2020]. The long-run average outcome is computed under the ground-truth data-generating process, and the stationary distribution is obtained from the transition matrix derived in Section B.

In the online customer-support experiment, we again search over threshold policies, but impose an additional monotonicity constraint on the induced marginal admission probability. Specifically, writing $\bar{\pi}(k) = \mathbb{P}[\pi(X_i, k) = 1]$, we require $\bar{\pi}(k_1) \leq \bar{\pi}(k_2)$ whenever $k_1 \geq k_2$. This constraint is not required by Theorem 4; it is used only to stabilize the finite-dimensional oracle search and to rule out highly oscillatory threshold vectors. The resulting policy should therefore be interpreted as an approximate oracle benchmark within this constrained threshold class. The constrained optimization is carried out using COBYLA, a derivative-free method for nonlinear optimization with inequality constraints [Powell, 1994, 1998], as implemented in `scipy.optimize.minimize` [Virtanen et al., 2020].

C.2 Offline Training and Policy Evaluation

For the learned-policy comparisons, all methods are trained on the same offline trajectories within each simulation replication. The performance boxplots in Figures 3 and 5 are based on 100 independent simulation replications for each sample size or observation horizon. Learned policies are evaluated under the ground-truth data-generating process to obtain their long-run average outcome or reward rate. This ground-truth model is used only for oracle benchmarking and final policy evaluation; it is not used to train SACT, the direct CADE baseline, CQL, or FQL.

C.2.1 SACT and the Direct CADE Baseline

All causal forests used in the direct baseline and in SACT are fit with 500 trees. The direct baseline estimates the state-aware CADE and assigns treatment whenever the estimated CADE is positive. SACT uses the same CADE-estimation specification, but combines the estimated CADEs with state-specific continuation-value thresholds obtained from the state-level dynamic program.

For SACT, we use two-fold cross-fitting for the CADE and nuisance estimates entering the empirical Bellman operator. Because the observations come from dependent trajectories, we do not split adjacent observations by independently shuffling individual arrivals. Instead, folds are constructed from trajectory blocks. In the reported simulations, natural empty-system states are used to form regenerative blocks when available, and the resulting blocks are randomly assigned to the two folds.

The state-level transition kernels used by SACT are estimated from the offline data by empirical conditional transition frequencies. They are not replaced by ground-truth

transition matrices during training. In the emergency-department experiment, the state is the pair of queue lengths (K_{0i}, K_{1i}) , where K_{0i} is the regular-queue length and K_{1i} is the fast-track-queue length. In the customer-support experiment, the state is the human-agent queue length K_i . Relative value iteration is initialized at $V^{(0)} \equiv 0$ and recentered at an empty-system anchor state: $(K_0, K_1) = (0, 0)$ in the emergency-department experiment and $K = 0$ in the customer-support experiment. We iterate until the sup-norm change in the recentered value function is below 10^{-6} or until 2,000 iterations have been reached.

C.2.2 Reinforcement-Learning Baselines

For the reinforcement-learning baselines, FQI is implemented using the `mushroom_rl` implementation with 25 fitted-Q iterations and an `ExtraTreesRegressor` backend with 120 trees. Discrete CQL is implemented using `d3rlpy`, with a two-layer neural encoder with 64 hidden units per layer, 120 training epochs, learning rate 3×10^{-4} , batch size 128, and conservative penalty $\alpha = 0.2$.

Both CQL and FQI are trained on arrival-level decision tuples. In the emergency-department experiment, the state features are (X_i, K_{0i}, K_{1i}) . In the customer-support experiment, the state features are (X_i, K_i) . The next state is the state observed at the next arrival decision epoch. Service completions between arrivals determine the next queue length and, in the customer-support experiment, the elapsed calendar time, but service completions themselves are not treated as decision epochs for the offline learners.

In the emergency-department experiment, the arrival rate is constant, so no reward-rate correction is needed. The reinforcement-learning baselines are therefore trained directly on the realized outcome Y_i . Boundary constraints are imposed for all methods in this setting: if the fast-track queue is full, the policy routes the patient to the regular queue; if the regular queue is full, the policy routes the patient to the fast-track queue; and if both modeled queues are full, the arriving patient is not included as an admitted decision epoch. The same feasibility override is applied during data generation, policy learning, and policy evaluation.

For CQL and FQI, we report oracle-tuned discount factors. Specifically, we search over $\gamma \in \{0.95, 0.98, 0.99, 0.995, 0.999\}$ and, for each method and environment, report the value of γ with the best average ground-truth long-run performance across sample sizes and replications. This tuning selects $\gamma = 0.99$ for customer-support CQL, $\gamma = 0.999$ for customer-support FQI, $\gamma = 0.995$ for emergency-department CQL, and $\gamma = 0.99$ for emergency-department FQI, matching the legends in Figures 3, 5, S1, and S2. Because this tuning uses ground-truth long-run performance, it is favorable to the reinforcement-learning baselines and would not be available in a real offline-learning application.

C.2.3 Reward-Rate Implementation for the Customer-Support Experiment

For the customer-support experiment, the objective is the long-run reward rate $\theta(\pi) = \mathbb{E}_\pi[R_i] / \mathbb{E}_\pi[\Delta_i]$, where Δ_i denotes the elapsed calendar time between consecutive user-arrival decision epochs in the arrival-embedded implementation. We therefore use the Dinkelbach version of SACT described in Section 3. In the implementation, the reward CADE τ_R , the elapsed-time CADE τ_Δ , and the state transition kernels are estimated once from the offline data. The Dinkelbach loop then updates the transformed outcome $R_i - \theta\Delta_i$ without refitting the causal forests. We initialize θ at the empirical reward rate $\sum_i R_i / \sum_i \Delta_i$ computed on the training portion of the trajectory, and stop when the esti-

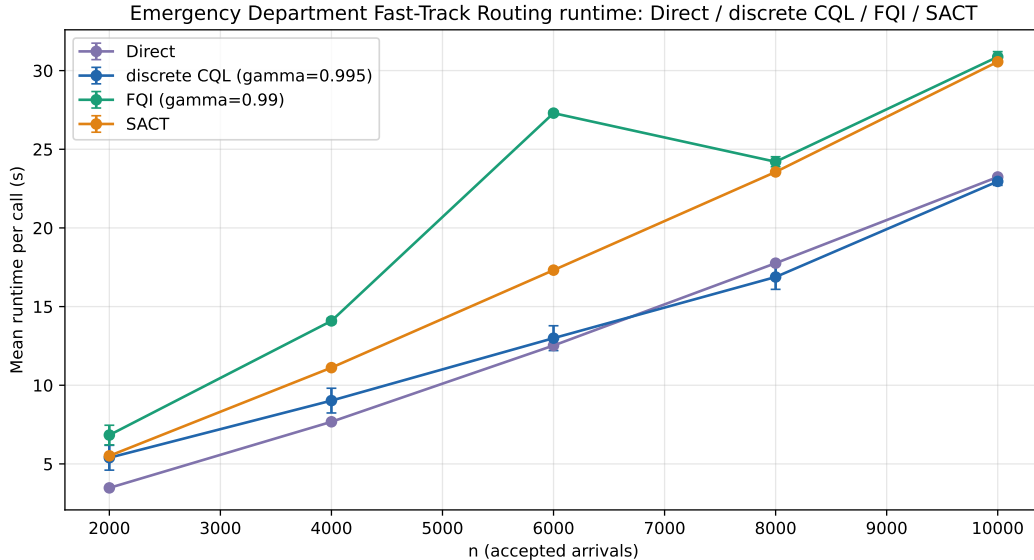


Figure S1: Runtime in the emergency-department fast-track routing experiment. The plot reports mean training time per call, excluding data simulation and evaluation. The gap between FQI and the other methods is much smaller than in the customer-support experiment because no reward-rate grid search is needed.

imated transformed average reward is below 10^{-5} in absolute value or after 50 Dinkelbach updates.

We adapt CQL and FQI to the same reward-rate objective by training them on transformed rewards $\tilde{R}_i(\rho) = R_i - \rho\Delta_i$ over a grid of candidate values of ρ . Let $\hat{\theta}_{\text{emp}} = \sum_i R_i / \sum_i \Delta_i$ denote the empirical reward rate computed on the training portion of the data. We use the five-point grid $\rho \in \{0, 0.5\hat{\theta}_{\text{emp}}, \hat{\theta}_{\text{emp}}, 1.5\hat{\theta}_{\text{emp}}, 2\hat{\theta}_{\text{emp}}\}$. We split the observed arrivals chronologically into a 70% training portion and a 30% validation portion. For each value of ρ , we train the off-the-shelf CQL or FQI learner on the transformed reward and select the policy with the largest validation estimate of $\theta(\pi)$. The validation estimate is computed by importance weighting using an estimated behavior policy $\hat{\pi}_0(X_i, K_i)$, clipped to $[0.05, 0.95]$. In the customer-support experiment, this estimated behavior model is allowed to depend on both user covariates and human-agent queue length, although the true status-quo policy specified in Section 4.2 depends only on user covariates.

C.2.4 Runtime Measurement

Runtime is measured as training time only and excludes data simulation, computation of the optimal policy benchmark, and evaluation. For reward-rate versions of CQL and FQI, the reported runtime includes training over the candidate ρ grid and selecting the final policy using the validation estimate described above.

Figure S1 reports runtime results for the emergency-department fast-track routing experiment. The methods have broadly comparable runtimes. FQI and SACT are somewhat more computationally expensive than the direct approach and discrete CQL, but they also

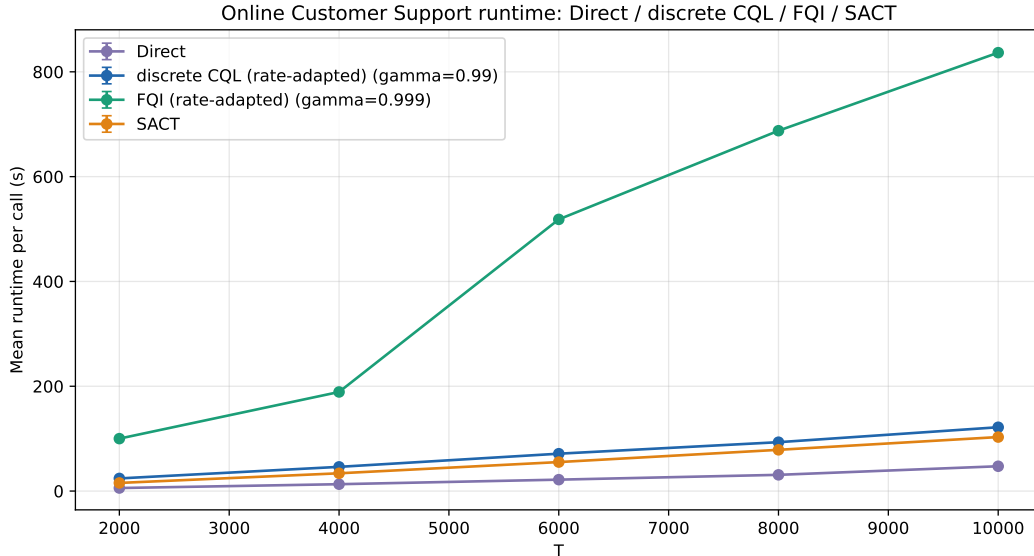


Figure S2: Runtime in the online customer-support experiment. The plot reports mean training time per call, excluding data simulation and evaluation. FQI is substantially slower than the other methods because the reward-rate adaptation requires retraining the full fitted-Q procedure over a grid of transformed rewards.

achieve stronger empirical performance in Figure 3.

Reported runtimes are single-CPU SLURM wall-clock times. Each configuration was submitted as a separate SLURM job, and the 100 replications within a configuration were executed sequentially on the same compute node. Because different configurations may run on different nodes, a small amount of hardware-induced variability remains in the reported runtimes. This variability is most visible for FQI, whose runtime is dominated by repeatedly fitting large tree ensembles. As a result, the FQI curve is not perfectly monotone in sample size; for example, the runtime at $n = 6000$ is slightly larger than at $n = 8000$. We view this as measurement noise arising from differences across compute nodes rather than a meaningful algorithmic phenomenon. Overall, runtime increases with sample size for all methods.

Figure S2 reports runtime results for the online customer-support experiment. All methods become more expensive as the observation horizon increases, but the increase is much sharper for FQI. This is mainly due to the reward-rate adaptation. For each candidate value of ρ , FQI runs a full sequence of fitted-Q iterations, and each iteration refits a 120-tree ensemble to Bellman targets based on the transformed reward $R_i - \rho \Delta_i$. Since the elapsed time Δ_i is state-dependent in the customer-support system, changing ρ can substantially change the scale and shape of the regression target. Thus, the five-point ρ sweep is especially costly for the tree-based FQI implementation. CQL is also retrained over the same grid, but its neural-network architecture and number of gradient steps are fixed, so the cost of each run is less sensitive to the transformed reward scale. SACT also solves the reward-rate problem iteratively, but its nuisance components are estimated once and reused across Dinkelbach updates, which keeps the runtime substantially below FQI.

D Proof of Theorems, Propositions, and Corollaries

D.1 Proof of Theorem 2

From Lemma 1, any deterministic policy π^* that satisfies

$$\pi^*(x, s) \in \operatorname{argmax}_{w \in \{0,1\}} \left\{ \eta_w(X, s) + \sum_{s' \in \mathcal{S}} P_{S,w}(s'|s) V^*(s') \right\} \quad (\text{S9})$$

for all $(x, s) \in \mathcal{X} \times \mathcal{S}$ is optimal. Note that for each fixed (x, s) , treatment is strictly preferred to control if and only if

$$\tau(x, s) + \sum_{s' \in \mathcal{S}} (P_{S,1}(s'|s) - P_{S,0}(s'|s)) V^*(s') > 0. \quad (\text{S10})$$

Equivalently, treatment is strictly preferred whenever $\tau(x, s) > c_s$, where

$$c_s = - \sum_{s' \in \mathcal{S}} (P_{S,1}(s'|s) - P_{S,0}(s'|s)) V^*(s') \quad (\text{S11})$$

At equality, the two actions have the same Bellman value, so choosing control still attains the maximum. Thus, the strict-threshold rule $\pi^*(x, s) = I(\tau(x, s) > c_s)$ attains the pointwise maximum and is optimal.

D.2 Proof of Theorem 4

Recall that the oracle policy thresholds the difference-of-Qs at zero:

$$\begin{aligned} \pi^*(x, s) &:= I(\delta^*(x, s) \geq 0), \\ \delta^*(x, s) &:= Q_{\pi^*}(x, s, 1) - Q_{\pi^*}(x, s, 0) \\ &= \tau(x, s) + \sum_{s' \in \mathcal{S}} \{P_{S,1}(s'|s) - P_{S,0}(s'|s)\} V^*(s'), \end{aligned} \quad (\text{S12})$$

with the differential Q-function under policy π defined as

$$Q_\pi(x, s, w) = \lim_{n \rightarrow \infty} \mathbb{E}_\pi \left[\sum_{i=1}^n (Y_i - \mu(\pi)) \mid X_1 = x, S_1 = s, W_1 = w \right] \quad (\text{S13})$$

The estimated policy can be written as

$$\hat{\pi}(x, s) := I(\hat{\delta}(x, s) \geq 0) \quad (\text{S14})$$

with

$$\hat{\delta}(x, s) := \hat{\tau}(x, s) + \sum_{s' \in \mathcal{S}} \{\hat{P}_{S,1}(s'|s) - \hat{P}_{S,0}(s'|s)\} \hat{V}^*(s'). \quad (\text{S15})$$

To bound the regret of $\hat{\pi}$, we first invoke the following performance-difference lemma for average-reward MDPs [Even-Dar et al., 2009, Jin et al., 2024], which expresses the value gap as an expectation under the stationary distribution of a single policy.

Lemma 6 (Performance Difference Lemma). *Let $Q_\pi(x, s, w)$ be defined as in (S13). Then for any two policies π and π' , the difference between their long-term average outcome is*

$$\mu(\pi') - \mu(\pi) = \mathbb{E}_{\pi'} [(\pi'(X, S) - \pi(X, S)) (Q_\pi(X, S, 1) - Q_\pi(X, S, 0))], \quad (\text{S16})$$

where the expectation is taken over $X \sim P_X, S \sim d_{\pi'}(S)$.

Recall that for any pair of (x, s) , $Q_{\pi^*}(x, s, 1) - Q_{\pi^*}(x, s, 0) = \delta^*(x, s)$. Thus, Lemma 6 implies that

$$\mu(\pi^*) - \mu(\hat{\pi}) = \mathbb{E}_{\hat{\pi}} [(\pi^*(X, S) - \hat{\pi}(X, S)) \delta^*(X, S)]. \quad (\text{S17})$$

For any fixed (x, s) , if $\pi^*(x, s) = 1$ and $\hat{\pi}(x, s) = 0$,

$$0 \leq \delta^*(x, s) \leq \delta^*(x, s) - \hat{\delta}(x, s); \quad (\text{S18})$$

on the other hand, if $\pi^*(x, s) = 0$ and $\hat{\pi}(x, s) = 1$,

$$0 \leq -\delta^*(x, s) \leq \hat{\delta}(x, s) - \delta^*(x, s). \quad (\text{S19})$$

Thus,

$$0 \leq (\pi^*(x, s) - \hat{\pi}(x, s)) \delta^*(x, s) \leq \left| \delta^*(x, s) - \hat{\delta}(x, s) \right|, \quad (\text{S20})$$

and

$$\begin{aligned} \mu(\pi^*) - \mu(\hat{\pi}) &\leq \mathbb{E}_{\hat{\pi}} \left[\left| \delta^*(X, S) - \hat{\delta}(X, S) \right| \right] \\ &\leq \max_{s \in \mathcal{S}} \left\| \delta^*(X, s) - \hat{\delta}(X, s) \right\|_{L_1(P_X)} \\ &\lesssim \max_{s \in \mathcal{S}} \|\tau(X, s) - \hat{\tau}(X, s)\|_{L_2(P_X)} + \left\| \hat{V}^* - V^* \right\|_\infty \\ &\quad + \max_{w \in \{0,1\}} \left\| \hat{P}_{S,w} - P_{S,w} \right\|_{\infty,1} \|V^*\|_\infty. \end{aligned} \quad (\text{S21})$$

By Lemma 3,

$$\begin{aligned} \left\| \hat{V}^* - V^* \right\|_\infty &\lesssim (t_0 + t_{\text{mix}}) \left(\|\hat{r}_0 - r_0\|_\infty + \max_{s \in \mathcal{S}} \|\hat{\tau}(\cdot, s) - \tau(\cdot, s)\|_{L_2(P_X)} \right) \\ &\quad + M_Y (t_0 + t_{\text{mix}})^2 \max_{w \in \{0,1\}} \left\| \hat{P}_{S,w} - P_{S,w} \right\|_{\infty,1} + \mathcal{O}_P \left(|\mathcal{I}_e|^{-1/2} \right). \end{aligned} \quad (\text{S22})$$

By Assumption 2, $|\mathcal{S}|$ is finite. Under the overlap condition in Assumption 4, each state-action pair (s, w) is visited with positive stationary probability under the behavior policy. Therefore, by standard root- n convergence of finite-dimensional empirical averages,

$$\max_{w \in \{0,1\}} \left\| \hat{P}_{S,w} - P_{S,w} \right\|_{\infty,1} = \mathcal{O}_P(|\mathcal{I}_t|^{-1/2}). \quad (\text{S23})$$

For estimating r_0 , define

$$\bar{r}_0(s) := \mathbb{E} \left[\hat{\eta}_0(X_i, s) + \frac{I(W_i = 0)}{1 - \hat{\pi}_0(X_i, s)} \{Y_i - \hat{\eta}_0(X_i, s)\} \mid S_i = s, \mathcal{I}_t \right]. \quad (\text{S24})$$

Conditionally on the training sample used to estimate $\hat{\eta}_0(x, s)$ and $\hat{\pi}_0(x, s)$,

$$\begin{aligned}
& |\bar{r}_0(s) - r_0(s)| \\
&= \left| \mathbb{E} \left[\hat{\eta}_0(X_i, s) + \frac{1 - \pi_0(X_i, s)}{1 - \hat{\pi}_0(X_i, s)} \{ \eta_0(X_i, s) - \hat{\eta}_0(X_i, s) \} - \eta_0(X_i, s) \mid S_i = s, \mathcal{I}_t \right] \right| \\
&\leq \mathbb{E} \left[\left| \frac{\hat{\pi}_0(X_i, s) - \pi_0(X_i, s)}{1 - \hat{\pi}_0(X_i, s)} \{ \eta_0(X_i, s) - \hat{\eta}_0(X_i, s) \} \right| \mid S_i = s, \mathcal{I}_t \right] \\
&= \mathcal{O}_P(|\mathcal{I}_t|^{-1/2})
\end{aligned} \tag{S25}$$

by Assumption 4. Thus,

$$\begin{aligned}
|\hat{r}_0(s) - r_0(s)| &\leq |\hat{r}_0(s) - \bar{r}_0(s)| + |\bar{r}_0(s) - r_0(s)| \\
&= \mathcal{O}_P(|\mathcal{I}_e|^{-1/2}) + \mathcal{O}_P(|\mathcal{I}_t|^{-1/2}),
\end{aligned} \tag{S26}$$

where the first term is the empirical fluctuation of the state- s average in (12) and is $\mathcal{O}_P(|\mathcal{I}_e|^{-1/2})$ since each state has positive limiting frequency and the summands are bounded.

Putting everything together, as $|\mathcal{I}_t|, |\mathcal{I}_e| \asymp n$,

$$\begin{aligned}
\mu(\pi^*) - \mu(\hat{\pi}) &\lesssim \max_{s \in \mathcal{S}} \|\tau(X, s) - \hat{\tau}(X, s)\|_{L_2(P_X)} + \|\widehat{V}^* - V^*\|_\infty \\
&\quad + \max_{w \in \{0, 1\}} \|\hat{P}_{S, w} - P_{S, w}\|_{\infty, 1} \|V^*\|_\infty \\
&= \mathcal{O}_P\left(n^{-(\beta \wedge \frac{1}{2})}\right)
\end{aligned} \tag{S27}$$

D.3 Proof of Proposition 5

Recall that the oracle policy thresholds the difference-of-Qs at zero:

$$\begin{aligned}
\pi^*(x, s) &:= I(\delta^*(x, s) \geq 0), \\
\delta^*(x, s) &:= \eta_1(x, s) - \eta_0(x, s) + \sum_{s' \in \mathcal{S}} \{P_{S, 1}(s' \mid s) - P_{S, 0}(s' \mid s)\} V^*(s').
\end{aligned} \tag{S28}$$

In both cases, we obtain the estimated policy by thresholding an estimated oracle score at zero.

We start by specializing the exogenous-covariate approach to the tabular setting. For each $x \in \mathcal{X}$, $s \in \mathcal{S}$, and $w \in \{0, 1\}$, we estimate the conditional mean outcome $\eta_w(x, s)$ and the state transition kernels $P_{S, w}(s' \mid s)$ by empirical conditional frequencies, and estimate the marginal law P_X by its empirical distribution. We then form the plug-in CADE estimate $\hat{\tau}(x, s) = \hat{\eta}_1(x, s) - \hat{\eta}_0(x, s)$, together with a plug-in estimate $\hat{r}_0(s)$ for $r_0(s)$, and the corresponding plug-in Bellman equation:

$$(\hat{T}_{S, \text{tab}} v)(s) := \hat{r}_0(s) + \left(\hat{P}_{S, 0} v \right)(s) + \sum_{x \in \mathcal{X}} \hat{P}_X \left(\hat{\tau}(x, s) + \left((\hat{P}_{S, 1} - \hat{P}_{S, 0}) v \right)(s) \right)_+. \tag{S29}$$

This removes the additional empirical integration step that motivated the sample-splitting construction in the general case.

By (23), for each $(x, s) \in \mathcal{X} \times \mathcal{S}$ and $w \in \{0, 1\}$,

$$\mathbb{P}[X_i = x, S_i = s, W_i = w] = \mathbb{P}[W_i = w \mid X_i = x, S_i = s] \mathbb{P}[X_i = x, S_i = s] \geq \frac{\Gamma_1 \Gamma_2}{|\mathcal{X}| |\mathcal{S}|}. \quad (\text{S30})$$

Therefore, by Hoeffding's inequality,

$$\max_{w \in \{0, 1\}} \|\hat{\eta}_w - \eta_w\|_\infty = \mathcal{O}_p \left(\sqrt{\frac{|\mathcal{X}| |\mathcal{S}| \log(|\mathcal{X}| |\mathcal{S}|)}{n}} \right). \quad (\text{S31})$$

Similarly,

$$\max_{w \in \{0, 1\}} \|\hat{P}_{S,w} - P_{S,w}\|_{\infty, 1} = \mathcal{O}_p \left(|\mathcal{S}| \sqrt{\frac{\log(|\mathcal{S}|)}{n}} \right). \quad (\text{S32})$$

Since the expectation over X in the Bellman operator $\hat{T}_{S, \text{tab}}$ is now evaluated by finite summation, the additional empirical-integration term in Lemma 3 disappears. By Lemma 3 but replacing \hat{T}_S with $\hat{T}_{S, \text{tab}}$,

$$\begin{aligned} & \|\hat{V}^* - V^*\|_\infty \\ & \lesssim (t_0 + t_{\text{mix}}) \max_{w \in \{0, 1\}} \|\hat{\eta}_w - \eta_w\|_\infty \\ & \quad + M_Y (t_0 + t_{\text{mix}})^2 \max_{w \in \{0, 1\}} \|\hat{P}_{S,w} - P_{S,w}\|_{\infty, 1} \\ & = \mathcal{O}_P \left((t_0 + t_{\text{mix}}) \sqrt{\frac{|\mathcal{X}| |\mathcal{S}| \log(|\mathcal{X}| |\mathcal{S}|)}{n}} + (t_0 + t_{\text{mix}})^2 |\mathcal{S}| \sqrt{\frac{\log(|\mathcal{S}|)}{n}} \right). \end{aligned} \quad (\text{S33})$$

Thus,

$$\begin{aligned} & \|\delta^* - \hat{\delta}\|_\infty \\ & \leq \|\hat{\tau} - \tau\|_\infty + 2 \max_w \|\hat{P}_w - P_w\|_{\infty, 1} \|V^*\|_\infty + 2 \|\hat{V}^* - V^*\|_\infty \\ & = \mathcal{O}_P \left((t_0 + t_{\text{mix}}) \sqrt{\frac{|\mathcal{X}| |\mathcal{S}| \log(|\mathcal{X}| |\mathcal{S}|)}{n}} + (t_0 + t_{\text{mix}})^2 |\mathcal{S}| \sqrt{\frac{\log(|\mathcal{S}|)}{n}} \right), \end{aligned} \quad (\text{S34})$$

and the policy regret is of the same order by the performance difference lemma, Lemma 6, using a similar argument as in proof of Theorem 4:

$$\begin{aligned} & \mu(\pi^*) - \mu(\hat{\pi}) \\ & \lesssim \|\delta^* - \hat{\delta}\|_\infty \\ & = \mathcal{O}_P \left((t_0 + t_{\text{mix}}) \sqrt{\frac{|\mathcal{X}| |\mathcal{S}| \log(|\mathcal{X}| |\mathcal{S}|)}{n}} + (t_0 + t_{\text{mix}})^2 |\mathcal{S}| \sqrt{\frac{\log(|\mathcal{S}|)}{n}} \right). \end{aligned} \quad (\text{S35})$$

We then consider the collapsed-state benchmark. Similarly, in this tabular setting, we can estimate $\eta_w(z)$ and $P_w(z' \mid z)$ by empirical conditional means and transition frequencies.

Let $(\hat{\mu}^*, \hat{V}^*)$ solve the empirical Poisson equation with the empirical Bellman operator for the collapsed state variable:

$$(\hat{T}v)(z) := \max_{w \in \{0,1\}} \left(\hat{\eta}_w(z) + \sum_{z' \in \mathcal{X} \times \mathcal{S}} \hat{P}_{Z,w}(z' | z) v(z') \right), \quad (\text{S36})$$

We can then consider the corresponding plug-in policy

$$\begin{aligned} \hat{\pi}^{\text{col}}(z) &:= I \left(\hat{\delta}^{\text{col}}(z) \geq 0 \right), \\ \hat{\delta}^{\text{col}}(z) &:= \hat{\eta}_1(z) - \hat{\eta}_0(z) + \sum_{z'} \{ \hat{P}_1(z' | z) - \hat{P}_0(z' | z) \} \hat{V}^*(z'). \end{aligned} \quad (\text{S37})$$

This collapsed-state benchmark can be viewed as a special case of the exogenous-covariate formulation by introducing a degenerate covariate $U_i \equiv \star$ and taking the state variable to be $Z_i = (X_i, S_i)$. Then, the collapsed-state Bellman operator

$$(Tv)(z) := \max_{w \in \{0,1\}} \left\{ \eta_w(z) + \sum_{z' \in \mathcal{X} \times \mathcal{S}} P_w(z' | z) v(z') \right\}, \quad (\text{S38})$$

coincides with the state-level Bellman operator in (10) written for the pair (U_i, Z_i) , because the expectation over the degenerate variable U_i does nothing, the average baseline $r_0(z)$ becomes $\eta_0(z)$, the CADE $\tau(u, z)$ becomes $\eta_1(z) - \eta_0(z)$, and the transition kernel is now $P_{Z,w}$. Thus, Lemma 3 carries over exactly once s is replaced by z .

By construction, the collapsed-state benchmark is the same Bellman problem as in Lemma 3, with state variable $Z = (X, S)$, reward functions $\eta_w(z)$, and transition kernels $P_{Z,w}(\cdot | z)$. Thus, from Lemma 3 (but replacing \hat{T}_S with \hat{T}_Z),

$$\begin{aligned} \left\| \hat{V}^* - V^* \right\|_{\infty} &\lesssim (t_0 + t_{\text{mix}}) \max_{w \in \{0,1\}} \|\eta_w - \hat{\eta}_w\|_{\infty} \\ &\quad + M_Y (t_0 + t_{\text{mix}})^2 \max_{w \in \{0,1\}} \left\| \hat{P}_{Z,w} - P_{Z,w} \right\|_{\infty,1}. \end{aligned} \quad (\text{S39})$$

Again, by (23) and Hoeffding's inequality,

$$\max_{w \in \{0,1\}} \|\hat{\eta}_w - \eta_w\|_{\infty} = \mathcal{O}_p \left(\sqrt{\frac{|\mathcal{X}| |\mathcal{S}| \log(|\mathcal{X}| |\mathcal{S}|)}{n}} \right), \quad (\text{S40})$$

and

$$\max_{w \in \{0,1\}} \left\| \hat{P}_{Z,w} - P_{Z,w} \right\|_{\infty,1} = \mathcal{O}_p \left(|\mathcal{X}| |\mathcal{S}| \sqrt{\frac{\log(|\mathcal{X}| |\mathcal{S}|)}{n}} \right). \quad (\text{S41})$$

Thus, following the same argument as in proof of Theorem 4,

$$\begin{aligned} \mu(\pi^*) - \mu(\hat{\pi}^{\text{col}}) &\lesssim \left\| \delta^* - \hat{\delta}^{\text{col}} \right\|_{\infty} \\ &\lesssim \max_w \|\hat{\eta}_w - \eta_w\|_{\infty} + \max_w \left\| \hat{P}_{Z,w} - P_{Z,w} \right\|_{\infty,1} \|V^*\|_{\infty} + \left\| \hat{V}^* - V^* \right\|_{\infty} \\ &= \mathcal{O}_p \left((t_0 + t_{\text{mix}})^2 |\mathcal{X}| |\mathcal{S}| \sqrt{\frac{\log(|\mathcal{X}| |\mathcal{S}|)}{n}} \right) \end{aligned} \quad (\text{S42})$$

E Proof of Lemmas

E.1 Proof of Lemma 1

We first write the standard Bellman optimality equation for the Markov decision process whose full state is $Z_i := (X_i, S_i)$, since our model can be viewed as a Markov decision process with state Z_i . By the average-reward optimality equation for Markov decision process [Sutton and Barto, 2018], there exist an optimal average reward μ^* and a relative value function $V_Z^* : \mathcal{X} \times \mathcal{S} \rightarrow \mathbb{R}$ such that

$$\mu^* + V_Z^*(z) = \max_{w \in \{0,1\}} \left(\eta_w(z) + \int_{z' \in \mathcal{X} \times \mathcal{S}} P_{Z,w}(z' | z) V_Z^*(z') \right), \quad (\text{S43})$$

where $P_{Z,w}(z' | z)$ denotes the collapsed covariate-state transition kernel. Under Assumption 1, $P_{Z,w}(z' | z) = P_{S,w}(s' | s) P_X(x')$, and thus

$$\mu^* + V_Z^*(x, s) = \max_{w \in \{0,1\}} \left(\eta_w(x, s) + \int_{(x', s') \in \mathcal{X} \times \mathcal{S}} P_{S,w}(s' | s) P_X(x') V_Z^*(x', s') \right). \quad (\text{S44})$$

Defining $V^*(s) := \mathbb{E}_X[V_Z^*(X, s)]$ and taking expectation over X on both sides yield

$$\begin{aligned} \mu^* + V^*(s) &= \mathbb{E}_X \left[\max_{w \in \{0,1\}} \left(\eta_w(X, s) + \int_{(x', s') \in \mathcal{X} \times \mathcal{S}} P_{S,w}(s' | s) P_X(x') V_Z^*(x', s') \right) \right] \\ &= \mathbb{E}_X \left[\max_{w \in \{0,1\}} \left(\eta_w(X, s) + \sum_{s' \in \mathcal{S}} P_{S,w}(s' | s) V^*(s') \right) \right]. \end{aligned} \quad (\text{S45})$$

This proves the first claim of the lemma.

Next, consider any policy π that attains the pointwise maximum inside the expectation for each covariate-state pair (x, s) . Then,

$$\mu^* + V^*(s) = \mathbb{E}_X \left[\eta_{\pi(X,s)}(X, s) + \sum_{s' \in \mathcal{S}} P_{S,\pi(X,s)}(s' | s) V^*(s') \right]. \quad (\text{S46})$$

Multiplying both sides by the stationary distribution $d_\pi(s)$ and summing over $s \in \mathcal{S}$, we obtain

$$\begin{aligned} \mu^* + \sum_s d_\pi(s) V^*(s) &= \mathbb{E}_X \left[\sum_s d_\pi(s) \eta_{\pi(X,s)}(X, s) + \sum_s d_\pi(s) \sum_{s'} P_{S,\pi(X,s)}(s' | s) V^*(s') \right] \\ &= \mu(\pi) + \sum_{s'} d_\pi(s') V^*(s'). \end{aligned} \quad (\text{S47})$$

Thus, $\mu^* = \mu(\pi)$ and π must be an optimal policy.

E.2 Proof of Lemma 3

Recall that the state-level operator is defined as

$$(T_S v)(s) = r_0(s) + P_{S,0}v(s) + \mathbb{E}_X \left[\left(\tau(X, s) + (P_{S,1} - P_{S,0})v(s) \right)_+ \right]. \quad (\text{S48})$$

and empirical version of the operator used in the algorithm is

$$(\hat{T}_S v)(s) = \hat{r}_0(s) + \hat{P}_{S,0}v(s) + \frac{1}{|\mathcal{I}_e|} \sum_{i \in \mathcal{I}_e} \left(\hat{\tau}(X_i, s) + (\hat{P}_{S,1} - \hat{P}_{S,0})v(s) \right)_+. \quad (\text{S49})$$

Then (μ^*, V^*) and $(\hat{\mu}^*, \hat{V}^*)$ satisfy

$$\mu^* \mathbf{1} + V^* = T_S V^*, \quad \hat{\mu}^* \mathbf{1} + \hat{V}^* = \hat{T}_S \hat{V}^*. \quad (\text{S50})$$

Define an intermediate Bellman operator

$$(\tilde{T}_S v)(s) = \hat{r}_0(s) + \hat{P}_{S,0}v(s) + \mathbb{E}_X \left[\left(\hat{\tau}(X, s) + (\hat{P}_{S,1} - \hat{P}_{S,0})v(s) \right)_+ \right], \quad (\text{S51})$$

with $(\tilde{\mu}^*, \tilde{V}^*)$ satisfy

$$\tilde{\mu}^* \mathbf{1} + \tilde{V}^* = \tilde{T}_S \tilde{V}^*. \quad (\text{S52})$$

For any $v : \mathcal{S} \rightarrow \mathbb{R}$ and any $s \in \mathcal{S}$, since $u \mapsto u_+$ is nonexpansive,

$$\begin{aligned} \left| (\hat{T}_S v)(s) - (T_S v)(s) \right| &\leq \|\hat{r}_0 - r_0\|_\infty + \max_s \|\hat{\tau}(X, s) - \tau(X, s)\|_{L_2(P_X)} \\ &\quad + 3 \|v\|_\infty \max_{w \in \{0,1\}} \left\| \hat{P}_{S,w} - P_{S,w} \right\|_{\infty,1} + \left| (\hat{T}_S v)(s) - (\tilde{T}_S v)(s) \right|, \end{aligned} \quad (\text{S53})$$

where

$$\left| (\hat{T}_S v)(s) - (\tilde{T}_S v)(s) \right| = \mathcal{O}_P \left(\frac{1}{\sqrt{|\mathcal{I}_e|}} \right). \quad (\text{S54})$$

Thus

$$\begin{aligned} \left\| \hat{T}_S V^* - T_S V^* \right\|_\infty &\leq \|\hat{r}_0 - r_0\|_\infty + \max_s \|\hat{\tau}(X, s) - \tau(X, s)\|_{L_2(P_X)} \\ &\quad + 3 \|V^*\|_\infty \max_{w \in \{0,1\}} \left\| \hat{P}_{S,w} - P_{S,w} \right\|_{\infty,1} + \mathcal{O}_P \left(|\mathcal{I}_e|^{-1/2} \right). \end{aligned} \quad (\text{S55})$$

By Assumption 3, for any $s, \tilde{s} \in \mathcal{S}$,

$$\begin{aligned} |V^*(s) - V^*(\tilde{s})| &\leq \sum_{t \geq 0} \left| \mathbb{E}_{\pi^*} [r_{\pi^*}(S_t) | S_0 = s] - \mathbb{E}_{\pi^*} [r_{\pi^*}(S_t) | S_0 = \tilde{s}] \right| \\ &\leq 2M_Y \sum_{t \geq 0} \left\| P_{S,\pi^*}^t(\cdot | s) - P_{S,\pi^*}^t(\cdot | \tilde{s}) \right\|_{\text{TV}} \\ &\leq 4M_Y \left(t_0 + \sum_{t \geq t_0} e^{-t/t_{\text{mix}}} \right) \leq 8M_Y (t_0 + t_{\text{mix}}). \end{aligned} \quad (\text{S56})$$

Since $V^*(s_0) = 0$,

$$\|V^*\|_\infty \leq \text{span}(V^*) \leq 8M_Y(t_0 + t_{\text{mix}}). \quad (\text{S57})$$

Define the oracle and empirical policies

$$\begin{aligned} \pi^*(z) &\in \operatorname{argmax}_{w \in \{0,1\}} \{ \eta_w(x, s) + (P_{S,w}V^*)(s) \}, \\ \hat{\pi}(z) &\in \operatorname{argmax}_{w \in \{0,1\}} \{ \hat{\eta}_w(x, s) + (\hat{P}_{S,w}\hat{V}^*)(s) \}. \end{aligned} \quad (\text{S58})$$

Then,

$$\mu^* \mathbf{1} + V^* = r_{\pi^*} + P_{S,\pi^*}V^*, \quad \hat{\mu}^* \mathbf{1} + \hat{V}^* = \hat{r}_{\hat{\pi}} + \hat{P}_{S,\hat{\pi}}\hat{V}^*, \quad (\text{S59})$$

and thus

$$\begin{aligned} \hat{\mu}^* \mathbf{1} + \hat{V}^* &= \hat{r}_{\hat{\pi}} + \hat{P}_{S,\hat{\pi}}\hat{V}^* \\ &= \hat{r}_{\hat{\pi}} + \hat{P}_{S,\hat{\pi}}V^* + \hat{P}_{S,\hat{\pi}}(\hat{V}^* - V^*) \\ &\leq \hat{T}_S V^* + \hat{P}_{S,\hat{\pi}}(\hat{V}^* - V^*), \end{aligned} \quad (\text{S60})$$

because $\hat{T}_S V^*$ is the pointwise maximization over w evaluated at V^* . Subtracting $\mu^* \mathbf{1} + V^* = T_S V^*$ gives

$$(\hat{\mu}^* - \mu^*) \mathbf{1} + \hat{V}^* - V^* \leq (\hat{T}_S V^* - T_S V^*) + \hat{P}_{S,\hat{\pi}}(\hat{V}^* - V^*). \quad (\text{S61})$$

Iterating,

$$\hat{V}^* - V^* \leq \hat{P}_{S,\hat{\pi}}^h(\hat{V}^* - V^*) + \sum_{m=0}^{h-1} \hat{P}_{S,\hat{\pi}}^m \left((\hat{T}_S V^* - T_S V^*) - (\hat{\mu}^* - \mu^*) \mathbf{1} \right). \quad (\text{S62})$$

Note that at the anchor state s_0 , $\hat{V}^*(s_0) = V^*(s_0) = 0$. Subtracting $\hat{V}^*(s_0) - V^*(s_0)$,

$$\begin{aligned} \hat{V}^*(s) - V^*(s) &\leq \left[\hat{P}_{S,\hat{\pi}}^h(\hat{V}^* - V^*) \right](s) - \left[\hat{P}_{S,\hat{\pi}}^h(\hat{V}^* - V^*) \right](s_0) \\ &\quad + \sum_{m=0}^{h-1} \left(\left[\hat{P}_{S,\hat{\pi}}^m(\hat{T}_S V^* - T_S V^*) \right](s) - \left[\hat{P}_{S,\hat{\pi}}^m(\hat{T}_S V^* - T_S V^*) \right](s_0) \right), \end{aligned} \quad (\text{S63})$$

where we used $\hat{P}_{S,\hat{\pi}}^m \mathbf{1} = \mathbf{1}$ to cancel the term involving $(\hat{\mu}^* - \mu^*) \mathbf{1}$. By Assumption 3,

$$\begin{aligned} \hat{V}^*(s) - V^*(s) &\leq 4 \left(t_0 + \sum_{m \geq t_0} e^{-m/t_{\text{mix}}} \right) \left\| \hat{T}_S V^* - T_S V^* \right\|_\infty \\ &\leq 8(t_0 + t_{\text{mix}}) \left\| \hat{T}_S V^* - T_S V^* \right\|_\infty. \end{aligned} \quad (\text{S64})$$

For the other side, (S59) implies

$$\begin{aligned} \hat{\mu}^* \mathbf{1} + \hat{V}^* &= \hat{r}_{\hat{\pi}} + \hat{P}_{S,\hat{\pi}}\hat{V}^* \\ &\geq \hat{r}_{\pi^*} + \hat{P}_{S,\pi^*}\hat{V}^* \\ &= \hat{r}_{\pi^*} + \hat{P}_{S,\pi^*}V^* + \hat{P}_{S,\pi^*}(\hat{V}^* - V^*), \end{aligned} \quad (\text{S65})$$

because $\hat{\pi}$ is greedy for \hat{T}_S at \hat{V}^* . Subtracting $\mu^* \mathbf{1} + V^* = T_S V^*$ gives

$$(\hat{\mu}^* - \mu^*) \mathbf{1} + \hat{V}^* - V^* \geq (\hat{r}_{\pi^*} - r_{\pi^*}) + (\hat{P}_{S,\pi^*} - P_{S,\pi^*})V^* + \hat{P}_{S,\pi^*}(\hat{V}^* - V^*). \quad (\text{S66})$$

Iterating,

$$\hat{V}^* - V^* \geq \hat{P}_{S,\pi^*}^h(\hat{V}^* - V^*) + \sum_{m=0}^{h-1} \hat{P}_{S,\pi^*}^m \left((\hat{r}_{\pi^*} - r_{\pi^*}) + (\hat{P}_{S,\pi^*} - P_{S,\pi^*})V^* - (\hat{\mu}^* - \mu^*) \mathbf{1} \right). \quad (\text{S67})$$

Evaluating at s and s_0 and subtracting,

$$\begin{aligned} \hat{V}^*(s) - V^*(s) &\geq \left[\hat{P}_{S,\pi^*}^h(\hat{V}^* - V^*) \right](s) - \left[\hat{P}_{S,\pi^*}^h(\hat{V}^* - V^*) \right](s_0) \\ &\quad + \sum_{m=0}^{h-1} \left[\hat{P}_{S,\pi^*}^m \left((\hat{r}_{\pi^*} - r_{\pi^*}) + (\hat{P}_{S,\pi^*} - P_{S,\pi^*})V^* \right) \right](s) \\ &\quad - \sum_{m=0}^{h-1} \left[\hat{P}_{S,\pi^*}^m \left((\hat{r}_{\pi^*} - r_{\pi^*}) + (\hat{P}_{S,\pi^*} - P_{S,\pi^*})V^* \right) \right](s_0) \\ &\geq -4 \left(t_0 + \sum_{m \geq t_0} e^{-m/t_{\text{mix}}} \right) \left\| (\hat{r}_{\pi^*} - r_{\pi^*}) + (\hat{P}_{S,\pi^*} - P_{S,\pi^*})V^* \right\|_{\infty} \\ &\geq -8(t_0 + t_{\text{mix}}) \left(\|\hat{r}_{\pi^*} - r_{\pi^*}\|_{\infty} + \left\| \hat{P}_{S,\pi^*} - P_{S,\pi^*} \right\|_{\infty} \right). \end{aligned} \quad (\text{S68})$$

Note that for all $s \in \mathcal{S}$,

$$\hat{r}_{\pi^*}(s) - r_{\pi^*}(s) = \hat{r}_0(s) - r_0(s) + \mathbb{E}_X [\pi^*(X, s) (\hat{\tau}(X, s) - \tau(X, s))] + \mathcal{O}_P \left(|\mathcal{I}_e|^{-1/2} \right). \quad (\text{S69})$$

Thus,

$$\|\hat{r}_{\pi^*}(s) - r_{\pi^*}(s)\| \leq \|\hat{r}_0 - r_0\|_{\infty} + \max_s \|\hat{\tau}(X, s) - \tau(X, s)\|_{L_2(P_X)} + \mathcal{O}_P \left(|\mathcal{I}_e|^{-1/2} \right), \quad (\text{S70})$$

and

$$\begin{aligned} \hat{V}^*(s) - V^*(s) &\geq -8(t_0 + t_{\text{mix}}) \left(\|\hat{r}_0 - r_0\|_{\infty} + \max_s \|\hat{\tau}(X, s) - \tau(X, s)\|_{L_2(P_X)} \right. \\ &\quad \left. + \|V^*\|_{\infty} \max_{w \in \{0,1\}} \left\| \hat{P}_{S,w} - P_{S,w} \right\|_{\infty,1} \right) + \mathcal{O}_P \left(|\mathcal{I}_e|^{-1/2} \right). \end{aligned} \quad (\text{S71})$$

Putting everything together,

$$\begin{aligned} \left\| \hat{V}^* - V^* \right\|_{\infty} &\lesssim (t_0 + t_{\text{mix}}) \left(\|\hat{r}_0 - r_0\|_{\infty} + \max_{s \in \mathcal{S}} \|\hat{\tau}(X, s) - \tau(X, s)\|_{L_2(P_X)} \right) \\ &\quad + M_Y (t_0 + t_{\text{mix}})^2 \max_{w \in \{0,1\}} \left\| \hat{P}_w - P_w \right\|_{\infty,1} + \mathcal{O}_P \left(|\mathcal{I}_e|^{-1/2} \right). \end{aligned} \quad (\text{S72})$$

E.3 Proof of Lemma 6

It follows directly from Lemma D.8 of [Jin et al. \[2024\]](#) that

$$\begin{aligned}\mu(\pi') - \mu(\pi) &= \mathbb{E}_{\pi'} [(\pi'(X, S) - \pi(X, S))Q_\pi(X, S, 1)] \\ &\quad \mathbb{E}_{\pi'} [((1 - \pi'(X, S)) - (1 - \pi(X, S)))Q_\pi(X, S, 0)] \\ &= \mathbb{E}_{\pi'} [(\pi'(X, S) - \pi(X, S)) (Q_\pi(X, S, 1) - Q_\pi(X, S, 0))],\end{aligned}\tag{S73}$$

where the expectation is taken over $X \sim P_X, S \sim d_{\pi'}(S)$, as the covariates are generated i.i.d. from P_X .